



UNIVERSIDADE D  
COIMBRA

Idiris Mehamud Aliyi

**Metal Matrix Composites Reinforced with Diamond Particles.**

VOLUME 1

Dissertação no âmbito do Mestrado Conjunto Europeu em Tribologia de Superfícies e Interfaces orientada pelo Professor Doutor Bruno Trindade e apresentada ao Departamento de Engenharia Mecânica da Faculdade de Ciências e Tecnologia da Universidade de Coimbra

Julho de 2019



FCTUC FACULDADE DE CIÊNCIAS  
E TECNOLOGIA  
UNIVERSIDADE DE COIMBRA

DEPARTAMENTO DE ENGENHARIA MECÂNICA

## **Metal Matrix Composites Reinforced with Diamond Particles**

Submitted in Partial Fulfilment of the Requirements for the Degree of Master in  
Tribology of Surface and Interfaces

Author

**Idiris Mehamud Aliyi**

Advisor

**Professor Bruno Trindade**

Jury

President: - **Professor Albano Cavaleiro**  
Professor at University of Coimbra

Vowels: - **Doctor João Paulo Dias**  
Adjunct Director of Instituto Pedro Nunes (IPN)

**Doctor Emilio Furtus**  
Instituto Pedro Nunes (IPN)

In the framework of Joint European Master in Tribology of Surfaces and Interfaces

---



joint european master  
in tribology  
of surfaces and interf  
Ljubljana • Leeds • Coimbra • Luleå

**Coimbra, July 2019**

# Acknowledgments

I want to thank Pr. Bruno Trindade for initiating such an interesting project. Also, I would like to thank my supervisors, Pr. Bruno Trindade and Dr. Emilio Furtos, for their guidance, encouragement, and constant support during experimental work and composing of this thesis. Further, I would like to recognize the work and support of the other people that contributed to this project, Nelson Duarte and Carlos Patacas of IPN for all the technical contributions for this work, and Vipin Richhariya and Filipe Samuel of the University of Minho for the effort, time, and resources invested in this project.

I want to thank my committee, Albano Cavaleiro, and Joao Paulo Dias, for their valuable feedback on my work. Also, I would like to thank my friends, colleagues, the department faculty, and staffs for their involvement in my preparation during the last years. Finally, I'd like to thank the TRIBOS consortium for this great opportunity and the European Commission the funding provided.

## Abstract

Materials surface modification aims for the development of new material's surfaces through different methods to improve their structure, phase composition, tribological, physical and mechanical characteristics in addition to their chemical composition. Future of glass industry passes through solving the plunger surfaces modification to reduce friction and wear during blowing or pressing stage of production. This thesis aims to study the modification of plunger surfaces through the design of metal matrix composite material located on the surface of Cu-Be-Co substrate, reinforced with diamond particles, which surfaces will be functionalized with a low melting alloy to improve the adherence of diamonds. Metal matrix from Cu-Be-Co substrate's reinforced by of diamond particles with a low melting alloy of copper-tin-titanium.

Mechanical alloying through Ball milling technique has been simultaneously used to design the low melting Cu-Sn-Ti alloy and diamonds surface functionalization. The 4.81 gr of powder particles ( 10 % of diamonds, and the remain composition from 75% wt of Copper 15% wt of Ti, 10% of tin and 1-3% of stearic acid) have been mixed and alloyed into an 80 ml vessel. The substrate Cu-Be-Co surface's texturized by laser to produce a pattern on the surface as a matrix, then functionalized diamond particles will be introduced into the matrix by cold isostatic press and sintering. For interpretation of the result, the main experimental procedures have been investigated to characterize the properties of substrate (Cu-Be-Co), functionalized diamond particles (diamond + Cu-Sn-Ti +stearic acid) and the metal matrix's composites reinforced by diamond particles. Hardness testing, X-Ray Diffraction (XRD), Scanning Electron Microscopy (SEM), Energy Dispersive X-Ray Spectroscopy (EDS), and tribological testing Pin-on-disk tests performed as characterization techniques.

Despite the presence of a variety of oxides, the reinforced material exhibited better tribological performance than the unreinforced Cu-Be-Co when tested on a pin-on-disk. As a consequence, significantly reduces of wear resistance and coefficient of friction attained, up to 12 times lower wear rate and 11% reduce of COF respectively.

*Keywords: - metal matrix, mechanical alloying, surface texture, and plunger wear, friction.*

# Content

<b>Chapter one</b> .....	<b>1</b>
1.1.Introduction .....	1
1.2.Objective.....	3
1.3.Motivation.....	3
<b>Chapter two</b> .....	<b>4</b>
2. State of art.....	4
2.1 Glass Forming Operations.....	4
2.2 Plungers.....	5
2.3 Copper-Beryllium.....	7
2.4 Metal matrix and Reinforcement composites .....	8
2.4.1. Microstructure of MMCs.....	9
2.4.2 Copper based Metal matrix composites (MMC) .....	10
2.4.3 Titanium-based metal matrix composites (MMCs) .....	11
2.4.4 Diamond reinforcement .....	11
2.4.5 Application of MMC.....	13
2.5 Basic methods.....	14
2.5.1 Mechanical Alloying.....	14
2.5.2 Surface Texturing in Tribology.....	15
2.5.3 Laser Surface texturing.....	18
2.5.4 Cold isostatic press and sintering .....	18
<b>Chapter Three</b> .....	<b>20</b>
<b>3. Methodology</b> .....	<b>20</b>
3.1.Sample preparation.....	20
3.1.1. Heat treatments.....	21
3.1.2. Functionalization of diamond particles.....	22
3.1.3. Surface Texturing .....	23
3.1.4. Incorporation and Consolidations of functionalized diamond into pattern .....	23
3.2.Characterization techniques .....	24
<b>Chapter Four</b> .....	<b>26</b>
<b>4. Result and Discussion</b> .....	<b>26</b>
4.1 . Effect of temperature and time on the microstructure and hardness of the Cu-Be-Co alloy..	26
4.2 .Functionalization of diamond particles.....	31
4.3 .Texturing of the Cu-Be-Co substrate.....	37
4.4 . Consolidation of the functionalized diamond particles.....	39
4.5 . Tribological testing.....	41
<b>Chapter Five</b> .....	<b>46</b>
<b>5. Conclusion</b> .....	<b>46</b>

## List of figures

Figure .2.1: Glass manufacturing by pressing with (a) a single mold and (b) split mold.....	5
Figure.2.2 Gob feeding steps.....	6
Figure.2.3. Copper-Beryllium.....	7
Figure.2.4. Physical and mechanical properties of composites as compared with two most commonly used alloys, i.e., steel and aluminum.....	9
Figure.2.5. Variation of the friction coefficient and Wear for Cu–Ti <sub>2</sub> SnC composites as a function of Ti <sub>2</sub> SnC volume fraction: (a) worn at a sliding speed of 20 m min <sup>-1</sup> under a normal load of 10 N; (b) worn at a sliding speed of 20 m min <sup>-1</sup> under a normal load of 30 N; (c) worn at a sliding speed of 40 m min <sup>-1</sup> under a normal load of 10 N.....	11
Figure .2.6: The sample images of the 50 vol% diamond composites with varying Ti addition in the Cu matrix: (a) 0.2 at % Ti, (b) 0.3 at % Ti, and (c) 0.6 at % Ti.....	12
Figure.2.7. Engine and aircraft components.....	13
Figure .2.8 Mechanical seals.....	16
Figure.2.9. Friction change with textured and untextured surface.....	16
Figure.2.10 (a) Schematic diagram of the reciprocating sliding test performed on the MoS <sub>2</sub> dimple-reinforced WC/TiC/Co material. (b) COF as function of the cutting speed of the MoS <sub>2</sub> dimple-reinforced WC/TiC/Co (MHT1) and the bare WC/TiC/Co (MHT2 ).....	17
Figure.2.11. Schematic diagram of cold isostatic press and sintering .....	19
Fig.3.1. Mechanical alloying.....	21
Figure.3.2. Surface texturing .....	23
Figure.3.3. Reinforced matrix .....	23
Figure 3.4. Polished sample .....	23
Figure .3.5. Overall schematics of representation of activities .....	25
Figure 4.1 - XRD patterns of the Cu-Be-Co alloy after annealing at a) 1h and b) 25h for different temperatures.....	27
Figure 4.2 – graphs of precipitates size.....	27
Figure.4.3. SEM micrographs of untreated and annealed sample at different temperature and time.....	29
Figure 4.4 – Optical microscopy images of the untreated sample (a) and annealed sample at 550°C for 25h (b).....	29
Fig.4.5. Effect of the temperature and time of the heat treatments on .....	30
Figure.4.6.SEM micrographs of powder after mechanical alloying at 600 rpm.....	31
Figure 4.7 – Particle size distribution of the mixtures after mechanical alloying at 600 rpm for (a) 5h, (b) 10h and (c) 25h.....	32
Figure.4.8. XRD diffractograms of the mixtures milled at 600 rpm for different times.....	33
Figure.4.9 (a) SEM micrographs and (b) EDS maps distribution of powder after mechanical alloying at 600 rpm for 25.....	34
Figure.4.10. powder milled at 600 rpm for 25h after DTA/TGA. (a) DTA/TGA graph ,(b) DTA curves for cooling and heating step, (c) DTA curves for cooling and heating steps corresponds to	

range of 600 <sup>0</sup> C-800 <sup>0</sup> C,(d) the corresponding SEM micrographs after DTA/TGA and (e)XRD pattern after DTA/TGA. ....	36
Figure 4.11 - Optical profilometry images of the Co-Be-Co textured samples. (a) 25% of the textured area and (b) 75% of the textured area. ....	37
Figure 4. 12. XRD diffractograms of Cu-Be-Co substrate and Textures Cu-Be-Co( as low incidence and 20 <sup>0</sup> XRD pattern substrate).....	38
Figure 4. 13. 3D and optical images of MMC,(a), 25% reinforced Sample. (b).25% reinforced samples ,(c),75% Reinforced Sample ,(d), 75% Reinforced Sample .....	39
Figure 4.14 Diffractogram of the reinforced sample corresponds to 25%.....	40
Figure 4.15: (a) Vickers hardness (5N) of bare Cu-Be and the MMC. (b) Image of one of the indentations made on the RCu-Be.....	40
Figure 4.16: COF during the tribological tests of unreinforced Cu-Be-Co (initial state and submitted to heat treatments and R-Cu-Be-Co.....	41
Figure 4.17. Sections were taken by 3D profilometer from the wear track corresponding with the samples: a) bare CuBe surface without annealing treatment, b) bare CuBe surface after annealing treatment, c) CuBe surface with a 25% of reinforcement and d) CuBe surface with a 75% of reinforcement. e) Full wear track of CuBe surface with 25% of reinforcement, f) Full wear track of CuBe surface with 75% of reinforcement.....	42
Figure 4.18. Wear track images from (a).25% and (b).75% reinforced samples.....	43
Figure 4.19: Profiles of the bare and reinforced Cu-Be after tribological testing.....	43
Figure 4.20: Diameter of the circular track on Soda lime ball and volume loss on wear track of samples due to the tribological testing.....	44
Figure 4.21 XRD diffractograms of unreinforced Cu-Be-Co after pin-on-disc and 25% reinforced -Cu-Be-Co after pin-on-disc .....	45

## List of Tables

Table 3.1. The details of the content of powder mixture for ball milling.....	21
Table 4.1. Hardness value at0.025N.....	38
Table 4.2. Wear Coefficient value.....	44

## Abbreviations

Ag	Silver
Al <sub>2</sub> O <sub>3</sub>	Aluminum oxide
COF	Coefficient of friction
Cu	Copper
Cu-Be	Beryllium copper (Cu-1.7Be wt. %-Co)
Cu-Be-Co	Beryllium copper (Cu-1.7Be wt. %-Co)
Cu-Sn-Ti	Copper-tin- titanium
DLC	Diamond-like carbon
DRC	Diamond-reinforced composite
DTA	Differential thermal analysis
EDS	Energy-dispersive X-ray spectroscopy
Fcc	Face centered cubic
Fe-Co	Iron cobalt
H-Cu Be	Heated treated copper beryllium
LS	Laser sintering
LST	Laser surface texturing
MA	Mechanical alloying
MMC	Metal matrix composite
MoS <sub>2</sub>	Molybdenum disulfide
Nd:YAG	Neodymium-doped yttrium aluminum garnet
PCA	Process controlling agent
PM	Powder metallurgy
R Cu-Be	Diamond-reinforced copper-beryllium
SEM	Scanning electron microscope
SiC	Silicon carbide
TGA	Thermogravimetric analysis
TiC	Titanium Carbide
Ti MMCs	Titanium based metal matrix composites
Ti <sub>2</sub> SnC	Titanium tin carbide
WC	Tungsten carbide
XRD	X-Ray diffraction

## Chapter 1

### 1.1. Introduction

From ancient time to recent years glass technology improved throughout time: at early stage producing ionic and covalent glasses depend on cooling rate and crystallization effect, recently replaced by the formation of magnificent transparent glass from metallic materials. These show the relevance and importance of glass study for a century [1].

Depending on the glass production route the glass from several compositions, structure, and different mechanical properties can be developed; for instance amorphous metallic glass from rapid solidification of metal vapors and atomic disordering of crystalline lattice [2], on the other hand lightweight glass container produced by “*press-and-blow*” method or “*blow and blow*” method [3].

Most of the glasses fabricated with highly automated and continuous processes, whereas a molten blend of silica and other compounds are shaped either by blowing or pressing. Accordingly, most of the glasses are still fabricated using a molten blend of silica and other compounds, which are molded either by blowing or pressing into a mold by a plunger. The plunger has direct contact with molten silica during blowing and pressing. In fact, temperature control and wear resistance are one of the main issues along pouring and distribution of the glass into a mold since it is an essential factor during the blowing and pressing steps.

Glass distribution, into a mold, is caused by glass deformation, which depends on the load used in the plunger and temperature of the mold. Furthermore, the adhesion between plunger and mold depend on the working temperatures and plunger surfaces. Therefore, control of these factors become a technological challenge when complicated, and lights shapes are made on glass [4].

By nature, glass is abrasive and hard material, in addition to this, the high temperature generated during production accelerates the wear of the plunger and proceed to surface oxidation and corrosion. Therefore properties of plunger surface profoundly affect the surface quality of the glass and plunger lifetime; because it has direct contact with molten glass to generate defect, friction, and wear. As well as, unbalanced or non-uniform distribution of temperature with glass surfaces

affect the cooling process of glass after molding. Particularly when plungers made of steel coated either with tungsten carbide (WC) or nickel (Ni) based materials used for pressing the produced glass and the plunger faces such challenges [5]. Gradually to decrease wear and allow better thermal conductivity the plunger made of copper-based and nickel-based alloys was introduced to the glass production industry [6]. In this work, the proposed reinforced metal matrix for plunger materials expected to reduce friction and wear, improve thermal conductivity and durability of plunger due to the presence of functionalized diamond contents and low melting alloy of copper on surfaces of plungers.

This innovative project proposes an alternative method to develop a metal matrix's composite (MMC) material, for the design of new plunger material able to meet desired quality of glass by packaging industry and to improve plunger life span. Metal matrix's composites allow compromised behavior of composite from two or more different properties of elements. Thus composites are capable of working at a higher - temperature than the limits of their base metal/substrate, also show improved strength, stiffness, thermal conductivity, friction coefficient, abrasion resistance, creep resistance, or dimensional stability [7].

This work focus on the improvement of life span and tribological properties of plunger's surfaces by developing reinforced metal matrix composite. Typically for improvement of such properties composites from carbon allotropes, chromium and copper are applicable. Metal matrix from copper and silicon carbide investigated at dry sliding wear show that increasing percentage of copper decrease wear rate [8].

To have better performance and incorporation of composites into the metal matrix, the surface texturing also play a vital role, as well as used to overcome adhesion and stiction. The experimental work present that laser-textured seal rings tested in oil, showing that the size spherical dimple shape can be optimized and the stiffness of the ring improved [9].

Finally, all possible approaches and arrangement of composites in metal matrix included as the task of this thesis work to develop desired metal matrix composite reinforced by diamond particles for optimizing properties of plunger material.

### 1.1. Objective

This project aims to improve tribological properties and lifetime of plunger used in the glass industry by proposing alternative material for substrate and designing surface modification. *Specifically*: - to improve the friction effect, wear resistance, corrosion, and life span.

### 1.2. Motivation

During the production of glass molding; heat flow management and surface properties of the plunger, are a crucial factor in reducing degradation, wear, abrasion and friction between glass, the wall of the mold and plunger during blowing or pressing. This heat flow and surfaces quality of plungers highly depend on plunger material composition used during the pressing process to create the desired shape of the mold. Therefore, the surface of plungers must modify to get high compactness of glass, long life span of the plunger, and better quality of glass. Consequently, this work aims that the metal matrix's surfaces of Cu alloy will be reinforced by diamond particles with the idea to produce a composite material at a superficial level. On this way, it is expected to increase the hardness and wear resistance, to decrease the friction coefficient and wear generation at high temperature.

Designing the reinforced metal matrix composites depends on desired properties of each content of composite materials, therefore to meet desired properties from composites; the property, weight, and phase of each substance or composition play a significant role. This project focuses on the development of a metal matrix composite material reinforced by diamond particles, which has previously been functionalized with brazing of low melting Cu-Sn-Ti alloy.

As an allotropic form of carbon, diamond exhibit high hardness and wear resistance, low thermal expansion, and excellent thermal conductivity. On the other hand, as copper presents high electrical and thermal conductivity; thereby, both materials are very useful for application where thermal control is fundamental to develop a heat transfer and heat dissipation. However, composite from two or fewer elements change only specific properties, in addition to copper to functionalize diamonds particles, other metal particles also considered. Accordingly, to enhance interface stability (binding ability) and performance of composite the tin, titanium, and stearic acid (to control phase) utilized during designing of low melting alloy.

The project aims to develop a novel metal matrix's composite (MMC) based on Cu-Be-Co substrate reinforced by functionalized diamond particles. The following work included: (1) Different particles size of diamond functionalized by low melting alloy Cu-Sn-Ti and stearic acid by mechanical alloying (MA), (2) The texturization of Cu-Be-Co as substrate by laser surface texturing to generate metal matrix (3) The incorporation and consolidation of the functionalized diamond particles to the metal matrix(plunger materials) by cold isostatic press and sintering.

To optimize the metal matrix's composite properties different controlling factors considered; such as particle size, content by weight, pressing power, pressure, and temperature of cold pressing, the milling time, milling speed, laser pulses, and the laser current are the main parameter used as controlling factors. The tasks have worked at University of Coimbra, Institute Pedro Nunes, University of Minho and at enterprise INTERMOLD.

## **Chapter Two**

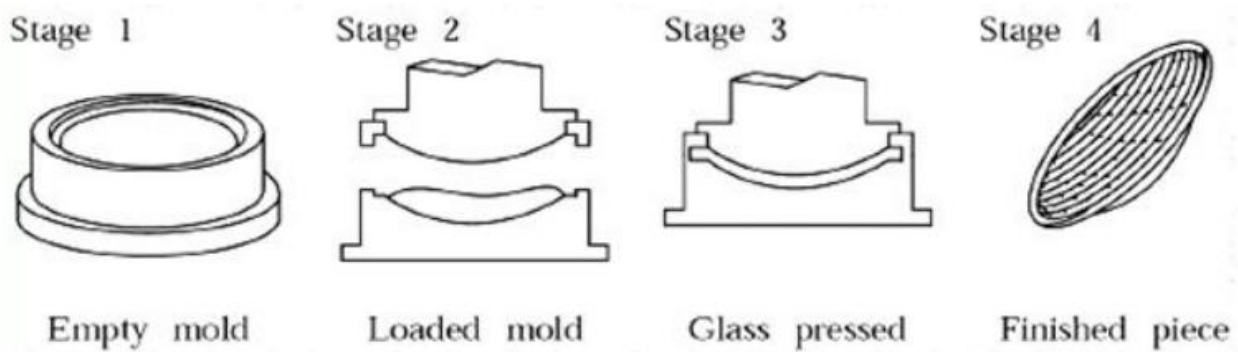
### **2. State of the art**

#### **2.1. Glass Forming Operations**

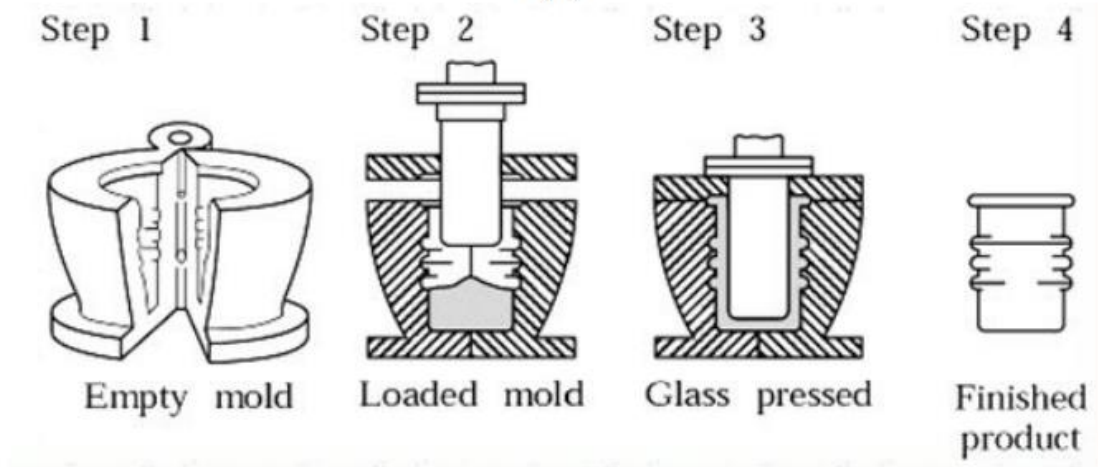
The glass manufacturing process can be divided into three different stages. The first one consists of the pouring of molten glass from the furnace to the mold. In the second one, the glass will adopt the designed shape by pressing or blowing process. Along with the third one, the glass subjected to an annealing process, during which temperature is cooling down slowly till room temperature. During this last stage, glass increases its stiffness, giving a final result, a hard solid glass with a low level of residual stresses.

Corrosion and wear flakes during blowing or pressing process affect the quality of glass and lifetime of plungers. Previously the plunger coated by nickel based matrix with hard particles to reduce friction, oxidation, and wear of plunger was used for blowing or pressing. Still, the plunger coated by nickel based matrix exhibit relatively small oxidation layer and less wear resistance and friction. This works improve the oxidation of plunger in addition to friction and wear during pressing or blowing stages. The pressing or blowing process is commonly used for the production

of culinary vessels, pots, lenses, and bricks, while the press-blown process is typically for goblets and light bottles [10].



(a)



(b)

Figure .2.1: Glass manufacturing by pressing with (a) a single mold and (b) split mold.

The production of desired shape and quality of glass depends on glass flow and heat transfer. Thereby, the thermal conductivity of molds and plungers plays an important role, since their surfaces are strongly affected by melted glass viscosity, which affects the final quality of glass.

## 2.2. Plungers

The pressing or blowing stage of glass into the mold during forming of shapes should avoid cracks, defect, porous and deformation of the glass surface, as well as should increases stability, production line productivity and quality of the final product. As discussed before, the quality and materials of plungers play a significant role for glass manufacturing in term of achieving the

desired shape of the glass and long life span of the plunger. Therefore optimizing plunger's material properties is crucial factors in the glass industry. Here below a schematic representation of glass mold processing for gob [11].

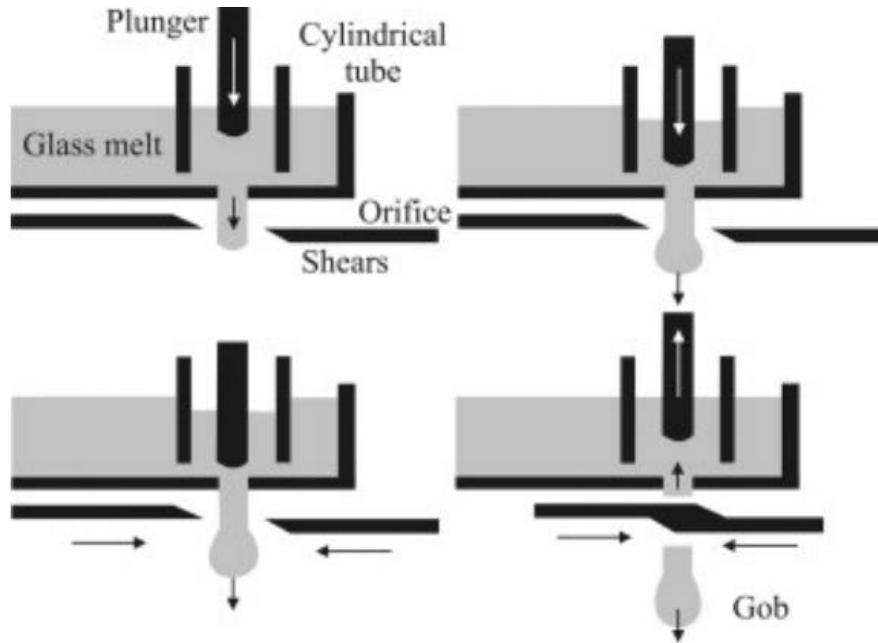


Figure.2.2 Gob feeding steps

On the other hand, plungers are exposed to harsh working conditions at high pressures and temperatures in corrosive environments. Even though for a short period, plungers are in direct contact with molten glass during processing. Thereby, plungers experience friction and wear, mostly due to adhesion and abrasion. Hence, the materials for these parts must meet the following requirements [12].

- Resistance to temperatures up to 650°C
- Stability under repeated thermal cycling
- Oxidation resistance
- Wear resistance
- Low thermal expansion
- High thermal conductivity

### 2.3. Copper- Beryllium

Beryllium copper alloy has extremely versatile application in the industry due to its unique characteristics. When copper is alloyed with up to 2% of Be and the resulting alloy is submitted to cold work and age treatments; the strength and hardness of the alloys are the highest in comparison with any other copper-based alloys. Consequently, the ultimate tensile strength increases up to 1.37 GPa. Moreover, this Cu-Be-Co alloy has better electrical conductivity, thermal conductivity, hardness, corrosive resistance, abrasive wear resistance, and better formability.

Nevertheless, the percentage of cobalt is low in the alloy; the cobalt increase wear resistance and lifetime of the plunger. This alloy is used to make bearings and pivoting elements for aircraft landing gear, fasteners, bushings and washers for tri-cone drilling bits, plastic forming molds, die casting plunger tips, safety tools, and cams [13, 14]. The glass industry use plungers produced from plain carbon steel, nickel-based alloy, or cast iron substrates [15]. This substrate relatively exhibits low hardness, low coating adhesion, less durability, and low wear resistance. These work propose Cu-Be-Co alloy as the substrate material for plungers uses in the glass production industry, to improve lifetime, thermal conductivity, and wear/friction resistance of plungers.



Figure.2.3. Copper-Beryllium

## 2.4. Metal Matrix and Reinforcement composites

The reinforced metal matrix composites are the process of mixing different material such as a polymer, ceramics, compound, and metal to generate third material with infinite variation and improved properties. The composites appear in the form of particles, whiskers, fibers, lamella or a mesh.

Matrix is a relatively ‘soft’ phase with an improvement of specific mechanical and physical properties, i.e., thermal conductivity, ductility, and formability. Reinforcement creates ‘Hard’ phase in between interfaces of the matrix to get high strength, stiffness, and low thermal expansion depend on the compositions. Therefore, the addition of reinforcements, which are usually stiffer than the matrix, allows designing composite materials able to withstand the high exerted load. Thereby, reinforcement improves strength, stiffness, or modifies the failure mechanism advantageously [16].

Metal matrix composites (MMCs) generally produced from low-density metal, such as titanium, copper, aluminum or magnesium are reinforced by particles, whiskers, lamella or fibers of ceramic material (CMC) or hard metal (such as silicon carbide or graphite). Reinforced metal matrix’s composite offer better performance in the following properties [17]:-

- ✓ Greater strength
- ✓ Improved stiffness
- ✓ Reduced density (weight)
- ✓ Improved high-temperature properties
- ✓ Controlled thermal expansion coefficient
- ✓ Thermal/heat management
- ✓ Enhanced and tailored electrical performance
- ✓ Improved abrasion and wear resistance
- ✓ Control of mass (especially in reciprocating applications)
- ✓ Improved damping capabilities.

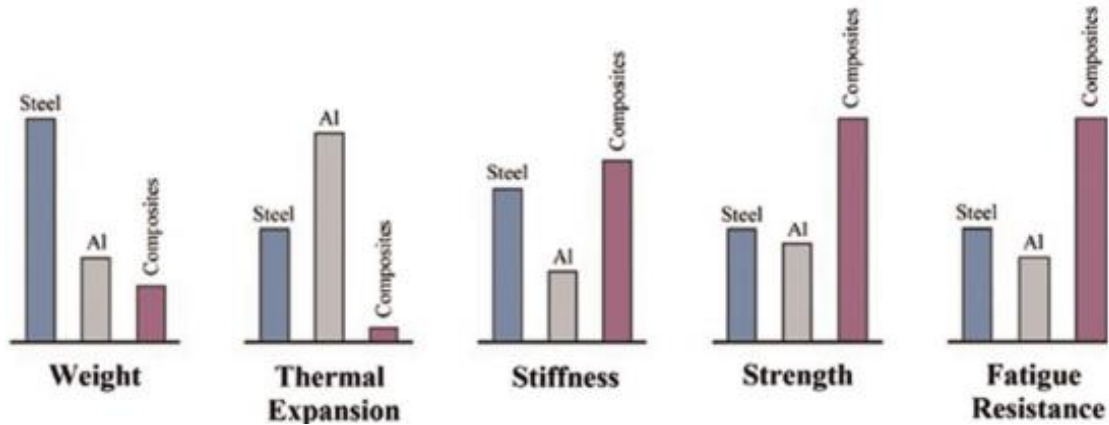


Figure.2.4. Physical and mechanical properties of composites as compared with the two most commonly used alloys, i.e., steel and aluminum.

Reinforced MMCs also show some disadvantages when compared with metals, such as a higher cost of fabrication [18]. Nowadays, the cost problem improved depend on the performance of composite (higher content of reinforcement gives higher performance efficiency, then require higher cost and vice versa). Further, designing the composite material located only on the surface of part of the bulk to reduce the cost of material consumption. For instance, diamond reinforced particles introduced to the metal matrix composite with a high content of diamond particles on bulk surfaces, which represent a new class of MMCs (metal matrixes composite) and mainly these project focus on it.

#### 2.4.1. Microstructure of MMCs

The different properties of metal matrix composite materials depend on microstructure and internal interfaces. The microstructures shown by metal matrix composites are related to the composition and how the reinforcement has been introduced into the metal matrix. The matrix from substrate/bulk contributes to microstructure as a source of chemical composition, grain and/or sub-grain size, texture, precipitation behavior, and lattice defects.

Reinforcement contributes as distribution of secondary reinforcing phases, grain size, and secondary phase of inter characteristics, and microstructural defects. Due to these factors, physical and mechanical properties of the reinforced composite materials are also strongly influenced by microstructures [19].

#### **2.4.2. Copper based Metal matrix composites (MMC)**

Cu exhibit high electrical and thermal conductivity; these factors make Cu an attractive material for several electrical and mechanical applications. Moreover, copper also shows high potential as a metal matrix for the design of composites to improve thermal conductivity and strength at high temperature. In fact, the use of Cu in the design of composite materials is quite old, since it was used to design the first one in 1950. From those initial, Cu based composite materials were possible to develop high strength at temperatures up to 925 °C (1700 °F) [20].

J. Sorensen, showed that the copper matrixes reinforced by Al<sub>2</sub>O<sub>3</sub> particles could exhibit exciting characteristics such as high thermal and electrical conductivity, as well as high strength and excellent annealing resistance [21]. Thereby, the selection of Cu based metal matrixes results interesting for their use in different applications of the industry such as; the design of resistance welding electrodes, lead frames and electrical connectors, materials for electronic packaging and thermal management applications with low thermal expansions coefficients and semiconductor materials.

The main challenge of metal matrices composite from pure copper is the reaction of copper with other metal at high temperature, which reduces the thermal conductivity of the metal matrices. But alloying Cu up to 2% by Be, reduces the reaction of copper at a higher temperature and improve the mechanical properties, corrosive resistance, and abrasive resistance [22]. Tribological behavior of Cu based metal matrix composite improved when reinforced by titanium and tin; typically coefficient of friction and wear rate reduced significantly as the contents of Ti<sub>2</sub>SnC particles increased (Figure.2.5) [23]. This is one of the concepts of these thesis work.

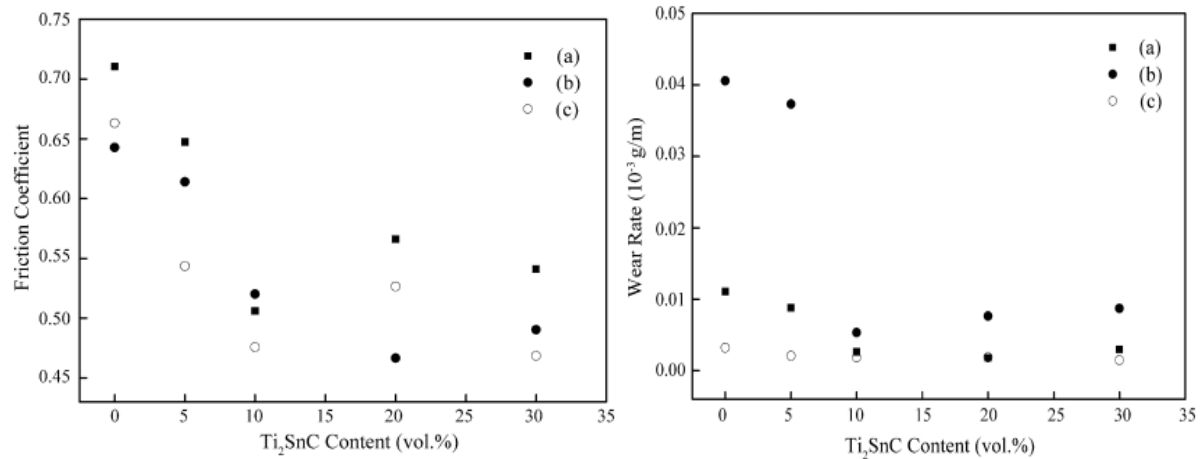


Figure.2.5. Variation of the friction coefficient and Wear for Cu–Ti<sub>2</sub>SnC composites as a function of Ti<sub>2</sub>SnC volume fraction: (a) worn at a sliding speed of 20 m/min–1 under a normal load of 10 N; (b) worn at a sliding speed of 20 m/min–1 under a normal load of 30 N; (c) worn at a sliding speed of 40 m/min–1 under a normal load of 10 N.

### 2.4.3. Titanium-based metal matrix composites (MMCs)

Titanium demands increase due to the need for lightweight and high-performance material in recent technology to have a lower density, compatibility, and higher strength. Ti MMCs demonstrate a higher mixture of fatigue, stiffness, specific strength, and creep resistance at raised temperatures [24]. Typically, Ti-MMCs are consumed for aerospace application when Titanium reinforced by continuous SiC fiber.

### 2.4.4. Diamond Reinforcement

Metal matrixes reinforced by diamond particles are a new and promising class of composite material in current development for tribological applications. Diamond is an inert material with unique properties, such as the highest thermal conductivity, high hardness, and high strength. These properties are the most interesting for the objectives of this project. Diamond has the highest thermal conductivity at room temperature of all existing materials ( $k = [800-2000]$  W m<sup>-1</sup> K<sup>-1</sup>), while relatively exhibit low thermal expansion [25]. Also for improving the performance of diamonds; the diamond particles functionalized by other metal such as copper and titanium. Mainly reinforcement of diamond particles with copper attracts many research works in

the recent time since copper has a better coefficient of thermal expansion, lower density, and higher thermal conductive.

Nowadays, the demands of thermal management materials are on the rise with thermal conductivity above 200W/mK [26]. The utilizing of high thermal conductive materials designed from diamond reinforcements introduced to heat sink component for different purpose and equipment, for instance, as hot pressing and gas pressure infiltration [27]. Similarly, these work aim to develop heat sink component for pressing of glass mold mainly plunger.

One of the main challenges that present the use of diamond particles as reinforcement is related to the difficulty of producing bulk MMC due to weak interface between diamond and metal as a consequence of poor wettability of diamond particles [28]. Therefore, to increase the adherence between diamonds and metal matrix, a functionalized diamonds by metals or alloys with high thermal conductivity, such as Cu, Ag, and Al have to be used [29]. The different method has been analyzed to improve diamonds wettability such as fabrication of matrix reinforcement under high pressure and high temperature [30].

Another method is the formation of carbides layer between diamond and metal interface to improve the wettability of diamond, for instance, using tungsten and titanium. The research work presents that in terms of thermal conductivity, the combination of diamond/copper matrixes show a better result from tungsten and/or titanium while titanium used as carbide layers or metallic binders [31]. Here the below figure shows the improvement of composite structure depend on the percentage of titanium, thus relatively as titanium percentage increases the structure of composite show better interface and uniform structure.

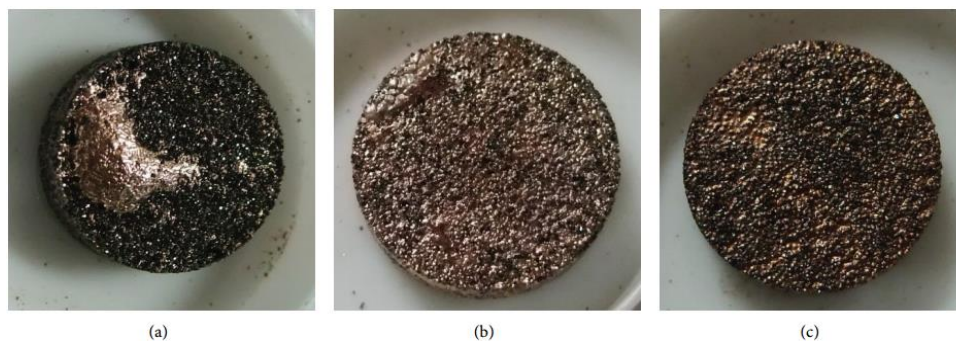


Figure .2.6: The sample images of the 50 vol% diamond composites with varying Ti addition in the Cu matrix: (a) 0.2 at % Ti, (b) 0.3 at % Ti, and (c) 0.6 at % Ti

On the other hand, matrixes reinforced by diamonds can improve tribological properties due to hardness and inertness of diamonds. The influence of different factors on the abrasive wear behavior of a diamond-reinforced Fe-Co composite was statistically studied [32], concluding that load and wear track are the significantly more determinant for this effect than hardness and sliding distance.

#### 2.4.5. Application of MMC

Composite material provides desirable properties depend on the composition and fabrication method of composites. Therefore owes different application in a different industry, commonly used for the following areas.

- ✓ Aerospace
- ✓ Transportation
- ✓ Electronics
- ✓ Electric power transmission
- ✓ Recreational products and sporting goods
- ✓ Wear-resistance material

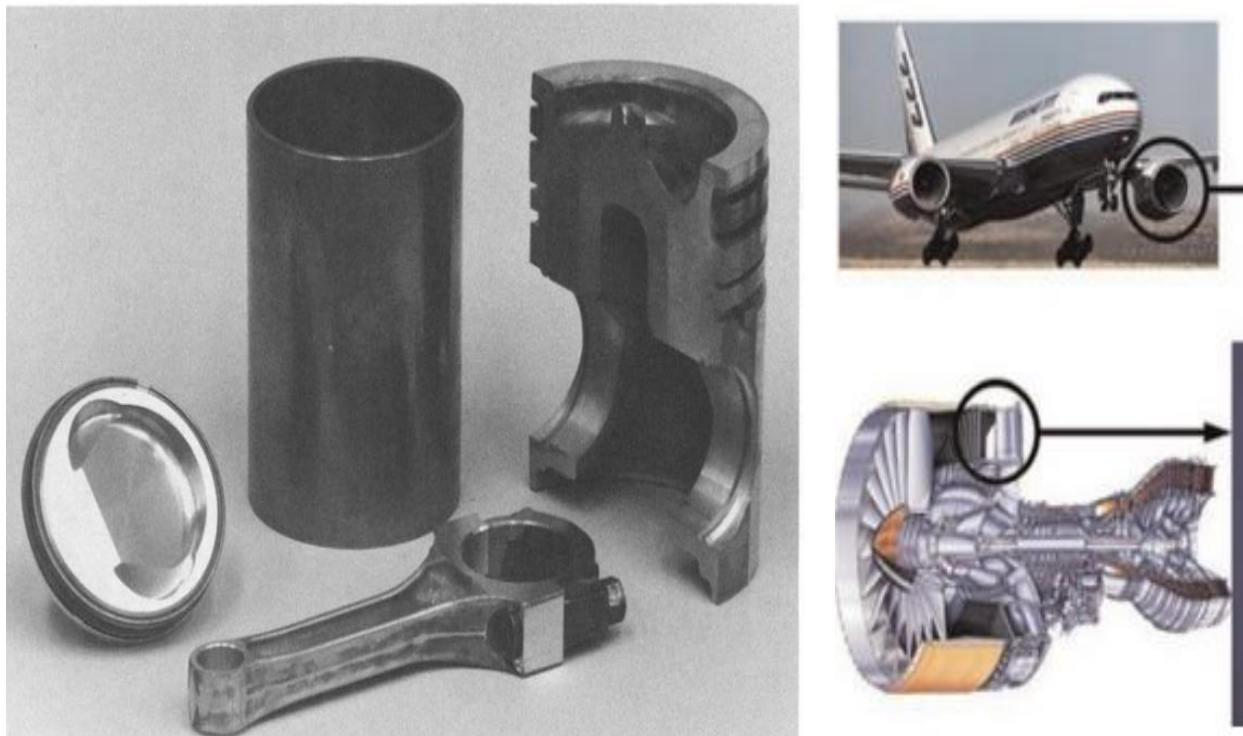


Figure.2.7. Engine and aircraft components

## 2.5. *Basic Methods*

Different mechanical and thermal mechanism included as production methods for sample preparations. These work related to the process of milling for the production of alloy, surface texturing, and cold press and sintering.

### 2.5.1. *Mechanical Alloying*

Mechanical alloying usually related to the milling process; the process of milling considered as breaking or reducing of course material to fineness level, for instance, production of fine powder particles (less than 70 micrometer). Mechanical alloying is a high energy milling technique with the aid of ball made up of different material, especially from steel. The mechanism widely applied for various engineering purposes at powder state. The MA process invented in 1966, at The International Nickel Company (INCO) to produce material for gas turbine application, under combining of oxide dispersion strengthening with gamma prime precipitation hardening in a nickel-based superalloy [33]. Over the past few decades, ball milling has evolved as a standard technique in material science and metallurgy.

Mechanical alloying through repeated fracturing and rewelding process of powder particles by ball mill under high energy, provide refinement particle size, different crystalline size, amorphous phases, deformed bonds at surfaces and changes in boundary energies. Therefore these process cause changes in the free energy which affect the reactants and the kinetics reaction of the composition in the composite [34]. Consequently, the process enhances solid-state reaction to take place between the fresh powder surfaces of the reactant materials at room temperature. These create a chance to produce alloys and compounds that are difficult or impossible to achieve by the conventional melting and casting techniques.

There are different factors that play significant roles and affect the mechanical alloying process to produce desired and homogeneous alloys/composites [35]. Sometimes, these factors considered as variables of production process parameters or process control agent (PCA). The primary need for process controlling agents is to avoid damages, unnecessary product, and establish a proper environment of milling. The common factors are the following:-

- ✚ Mill media:- ball or rods
- ✚ Milling environment:- vacuum, nitrogen, air or inert gas
- ✚ The ratio of ball size
- ✚ The ratio of the ball to powder size
- ✚ Milling time
- ✚ Milling temperature
- ✚ Catalyst:- another ingredient like stearic acid

Previous experimental work analysis shows that a higher PCA content leads to a higher yield. On the other hand, PCA is added into powder mixture by weight between 1- 5 wt.% of the total powder used as a catalyst [36]. Similarly observed that the effect of stearic acid on high energy milling of mechanical alloying, which conclude that density of sample increased without the addition of stearic acid while density decreased as stearic acid added to the powder mixtures [37].

Milling time affects different characteristics of composites. For instance as increasing the milling time from 1–50 h, the microhardness values of the hot pressed and hot extruded samples increase from  $51 \pm 2.26$  to  $155 \pm 6.5$  HV and from  $45.1 \pm 2.24$  to  $144 \pm 10.5$  HV, respectively and improve consolidation process for Al matrix composites reinforced with Fe based glassy particles [38]. The optimization of PCA will ensure a higher yield, proper composites, uniform structure, and short downtimes during milling.

### **2.5.2. Surface Texturing in Tribology**

Tribology plays a significant role in the optimization of surfaces in contact by adjusting friction and wear of the assembled components; this allows enhancing relative sliding motion and improving energy efficiency. For those tribological applications, where the exerted load is high, a soft substrate, which can be deformed plastically, can make to increase wear generation between surfaces under relative motion. There are different techniques used as a solution for this problem in tribology, but the laser surface texturing play key roles and widely applied method.

I. Etzion et al. present that laser surfaces texturing focused on improving lubrication regime of mechanical seals by varying dimple diameters, depth, and density with a different phase of experimental works, finally concluded the higher depth, density play the significant role than the real shape of micro dimples [42].

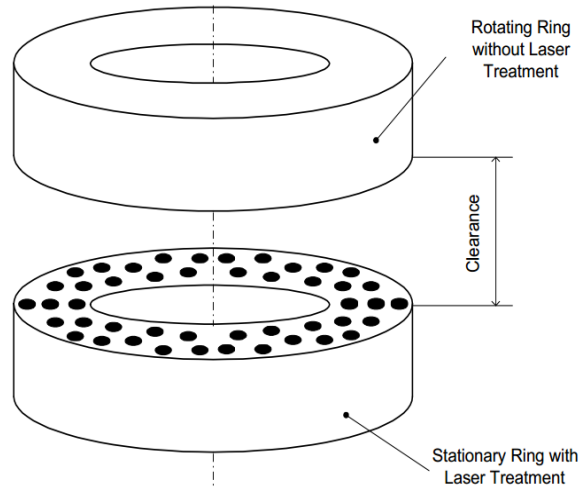


Figure .2.8 Mechanical Seals

Hu. Litian et al. analyzed the effect of laser surface texturing based on the diameter of texturing on a composite of titanium- aluminum –vanadium. Experimental work carried out with a sample of three different diameters and two oils with different viscosity. Finally, the result showed that the coefficient of friction was reduced for all textured surface when there were compared to the untextured surface [43].

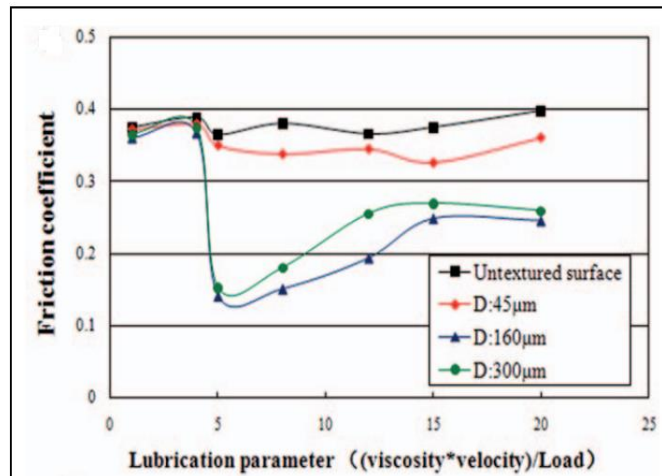


Figure.2.9. Friction change with textured and untextured surface

Similarly, an experimental investigation [44] developed a pattern of micro-holes on the surface of WC/TiC/Co cemented carbide by laser texturing. Then the dimples filled with MoS<sub>2</sub> and evaluated in the reciprocating sliding test (figure 2.10) and dry cutting test. Due to the formation of a self-lubricating film at the interphase and reducing the contact area, the material exhibited lower cutting forces, temperature, and COF than the bare WC/TiC/Co (figures 2.10).

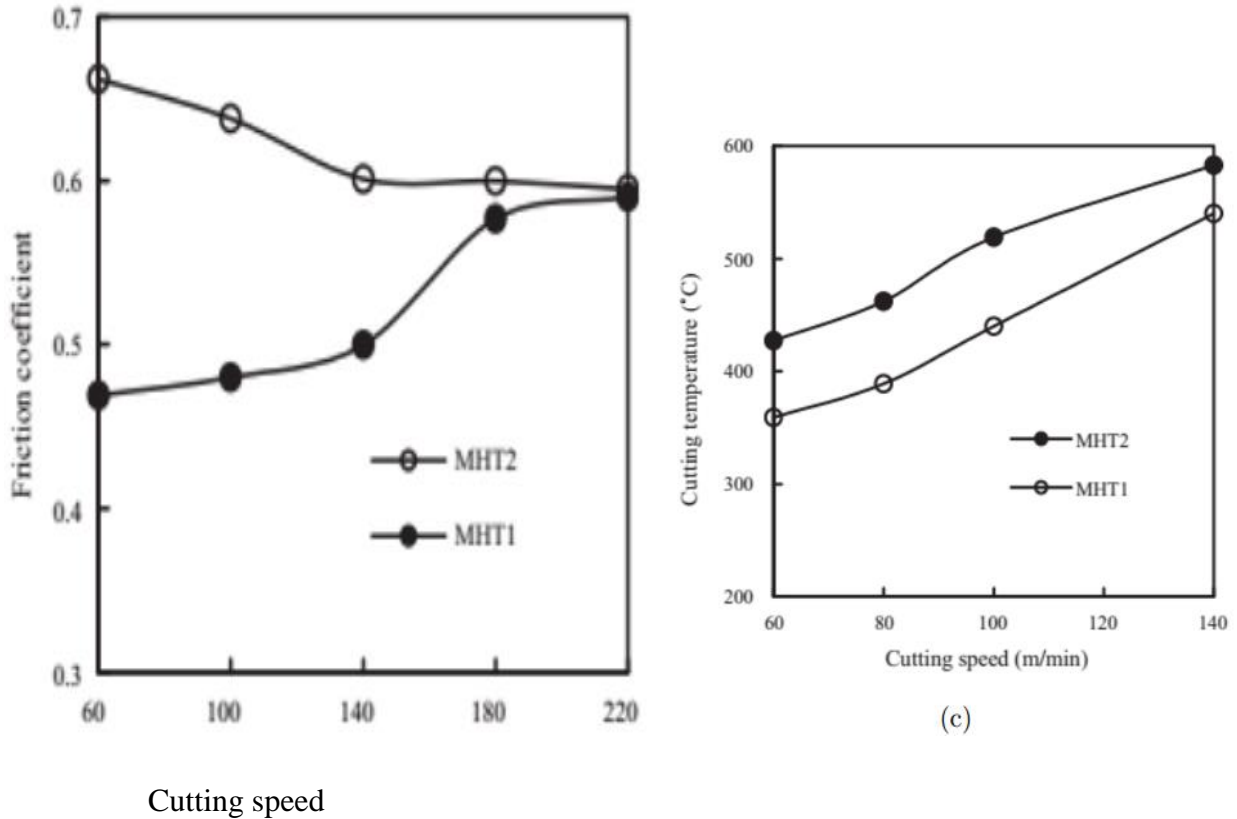


Figure.2.10 (a) Schematic diagram of the reciprocating sliding test performed on the MoS<sub>2</sub> dimple-reinforced WC/TiC/Co material. (b) COF as a function of the cutting speed of the MoS<sub>2</sub> dimple-reinforced WC/TiC/Co (MHT1) and the bare WC/TiC/Co (MHT)

### **2.5.3. Laser Surface texturing**

In tribology field, the development of a proper textured surface enhances the performance of the surface. This is also an alternative method in surface engineering for significant improvement in load capacity, the influence of geometry, better adhesion, wear resistance, friction coefficient, etc. Surface texturing has been determined as an innovative engineering solution to the surface that allows the way of enhancing the tribological performance of mechanical components [39].

Nowadays, different kinds of techniques are used for the development of textured surfaces such as machining, ion beam texturing, etching techniques, and laser surface texturing. From all of them, laser surface texturing is the most indicated for this project. Cylinder liner honing is the most familiar and earliest commercial application of a textured surface by laser [40]. Other similar application established the design to improve the hydrodynamic lubrication of bearings by surface texture [41].

Laser surface texturing is extremely fast, clean to the environment, and allow excellent control of the shape and size of the pattern. Laser surface texturing consume laser light as a source of power. Light frequency, spot rate, power source, and transverse speed are the parameters to control during the texturing process.

### **2.5.4. Cold isostatic press and sintering**

Powder metallurgy is an approximate shape manufacturing method that involves the incorporation and consolidation of powders particles into the desired shape — the system pressure and temperature cause particles to bond to each other. Thus imparting the necessary strength and metallurgical integrity to the manufactured part [45].

Cold isostatic press and sintering are one of the widely used methods in powder metallurgy to compact and sinter the powder together for the production of the desired shape. Also, this method used to manufacture products from a mixture of two or more types of metal powders to improve the mechanical properties and chemical properties of the new materials [46]. During cold isostatic press and sintering the heat treatments and die compaction of powder take places separately. The process experience high pressure during the cold press, and then high temperature. Metal powders

load in a die (usually graphite) at room temperatures for a period that can range from several minutes to an hour. Once pressure applied to the powder, the particles start to deform and enhance densification. Later the pre-weighted powder fed into the electric oven to sinter under high temperature. The cold isostatic press and sintering process depends on the following variables; time, temperature, and pressure, and influenced by particle size, shape, composition, and size distribution.

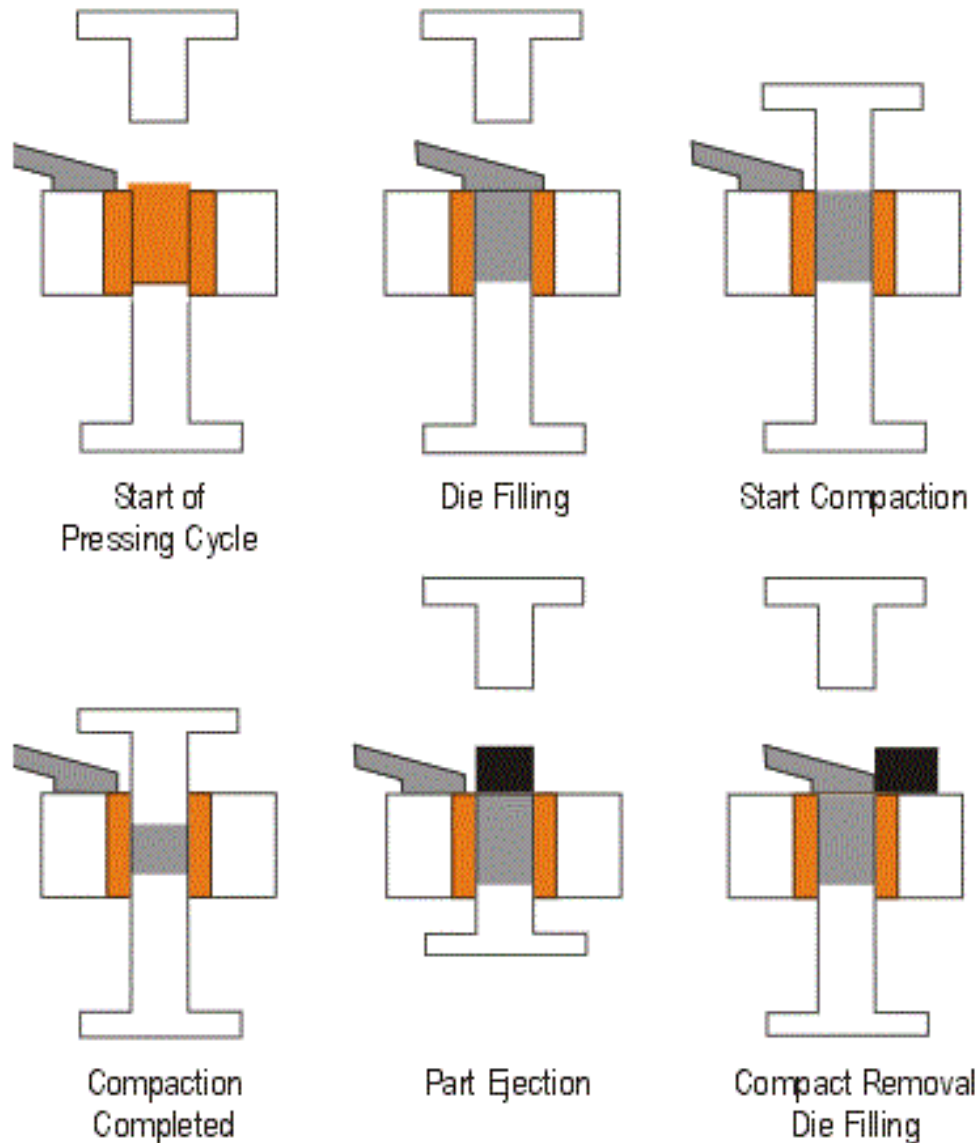


Figure.2.11. Schematic diagram of Cold isostatic press

## Chapter Three

### 3. Methodology

Different steps have been performed to design a surface modification in the form of metal matrix composite material; reinforcing the surface of Cu-1.7wt.%Be-Co alloy by functionalized diamonds particles. For that, first is necessary to develop a brazing alloy able to increase the adherence of diamonds on Cu-Be-Co alloy. Therefore, diamond particles have been mixed with Cu, Sn and Ti powders and alloyed by ball milling to functionalize diamonds surfaces with a brazing alloy able to increase their adherence. Likewise, Cu-Be-Co surface has been textured by laser to produce a 3D pattern, which will be filled with the functionalized diamonds. Finally, the incorporation of these diamonds to the Cu-Be-Co surface will be made at high pressure by cold isostatic press and sintering. During this processing route, brazing alloy will be melted to integrate diamonds into a 3D pattern. Once, surface modification complete, its tribological properties will be evaluated by a reciprocating pin-on-disc.

#### 3.1. Sample preparation

The main activities to prepare samples are ball milling, laser surface texturing, and cold isostatic pressing/sintering. Sample preparation needs the optimization of mechanical alloying, laser surface texturing, and hot pressing process since surface properties modification and optimization depend on different parameters related to these techniques.

##### 3.1.1. Heat treatments

During glass manufacturing operations, plunger is exposed to an abrasive wear and corrosion working conditions. In this harsh environment at temperatures as high as 600<sup>0</sup>C, mechanical properties shown an evolution as a consequence of initial  $\gamma''$  precipitates, developed during aged treatment, are dissolved in the Cu matrix, and new Cu-Be-Co precipices start to nucleate and grow up. This evolution produces a reduction of hardness, yield strength and corrosion resistance, and therefore lifespan of plunger. Therefore it's necessary to examine the development of hardness with the time and temperature through different annealing treatments (According to the Cu-Be-Co phase diagram, three different temperatures, 450<sup>0</sup>C, 550<sup>0</sup>C and 650<sup>0</sup>C and times ,during 1, 10 and 25 h, have been selected in order to study the evolution of GP,  $\gamma''$ ,  $\gamma'$ ,  $\gamma$ ,  $\beta$  and  $\alpha$  precipitates

present in Cu-1.7wt.%Be-Co alloy. Vickers hardness measurements will be made on untreated and treated samples and their values will be correlated with microstructure evolution through optical microscopy, scanning electron microscopy, SEM, and X-ray diffraction patterns, XRD.

### 3.1.2. Functionalization of diamond particles

Two different synthetic diamond sizes ( 0.5-1 and 15-25  $\mu\text{m}$ ) have been mixed with powders of Cu ( 99 wt.% purity), Ti ( 99.5 wt.% purity) and Sn (99.9 wt.% purity) with sizes of 50, 45 and 45  $\mu\text{m}$ , respectively, in a planetary ball mill [Fritsch Pulverisette 7]. For the milling, ten and twenty Cr-hardened steel balls, with diameters of 10 and 5 mm of diameter respectively, have been used together during milling time. Likewise, the ratio of a 1:10 ball-to-powder weight ratio was selected, this being 4.81 gr of powder and 48.1 gr of balls. Thereby, Cu-Sn-Ti powders were mixed with 10 wt.% of diamonds composed by 1/3 smaller and 2/3 bigger. The remaining amount of powder is composed 10 wt.% of Sn, 15wt.% of Ti and the rest Cu, together with stearic acid (1-3 wt.%), which is introduced to reduce the powder agglomeration. Two different speeds (200 and 600 rpm) have been evaluated at different times (5, 10, 25 and 30hr) to determine the better conditions to produce Cu solid solution. The details of this development are summarized in table 3.1

Mixture No	Mixture type	Stearic acid(% wt)	Diamond content(% wt)	Speed(rpm)	Time
1	Cu-10Sn-15Ti	3	10	200	5h
2	Cu-10Sn-15Ti	3	10	600	5h
3	Cu-10Sn-15Ti	3	10	600	10h
4	Cu-10Sn-15Ti	3	10	600	25h
5	Cu-10Sn-15Ti	3	10	600	30h

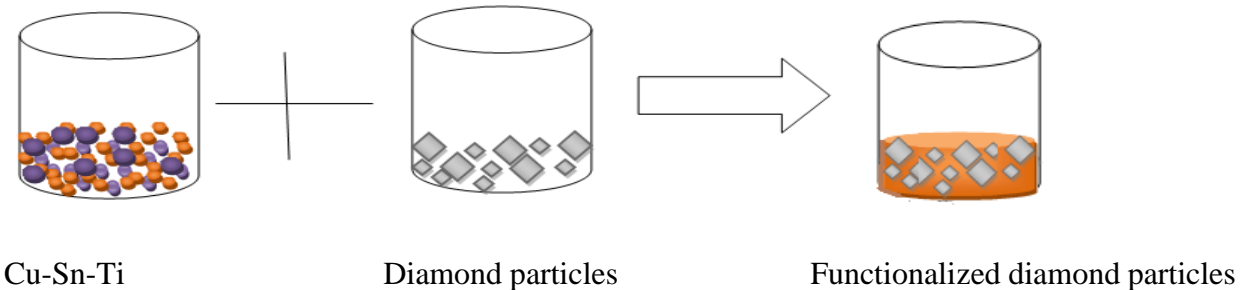


Fig.3.1. Mechanical Alloying

The processed powder characterized for their structure and efficiency. Powder evolution with milling time and speed has been putting attention to the crystallography, morphology and particle size evolution by Scanning Electron microscopy (SEM) [Zeiss Merlin] in secondary electrons detection model, X-ray Diffraction (XRD) [Philips X'Pert] and a laser scattering for particle size distribution analysis [Mastersizer 3000].

On the other hand, powder and diamond mixing will be subjected to high temperature during the sintering process. Therefore, their possible reactions and phase transformations as a function of the temperature must be evaluated. For that Differential Thermal Analysis (DTA) and Thermogravimetric Analysis (TGA) will be performed simultaneously. Thereby, the temperature of powders was increased up to 805°C at a rate of 10°C/min. The tests were carried out in a constant flow of Ar gas, established after reducing the chamber pressure to 7mbar, and such conditions were sustained until the cooling process was complete. After, the resulting powder characterized by XRD, SEM, and Energy-dispersive X-ray Spectroscopy (EDS) [Oxford Instruments X-MaxN].

### **3.1.3. Surface texturing**

A textured pattern in the form of squares has been generated on (Cu-1.7wt. %Be-Co) plates by laser to develop matrix on the surface of Cu-Be-Co plates. For that different parameter of an Nd: YAG laser [Sisma OEM 60 Plus, max. Power: 6W, wavelength: 1064 nm, speed (2-32m/s), laser power (25-100%)] was utilized in an open atmosphere of flowing Ar to create patterns. The patterns expected to have a dimension of 200 $\mu$ m depth with a square area of 200\*200 $\mu$ m and parallel arrangement to each other. The generated pattern evaluated by XRD [Oxford Instruments X-MaxN] and optical profilometry [Perthen Perthometer PRK].

A set of 4 samples in the form of discs with a diameter of 25mm and thickness of 6,75mm have been used for laser surface texturing. The textured surface was increased from 0 to 25% and 75%; by the percentage of surface area coverage. For instance, 25% of space will be produced between the pattern to be filled by functionalized particles.

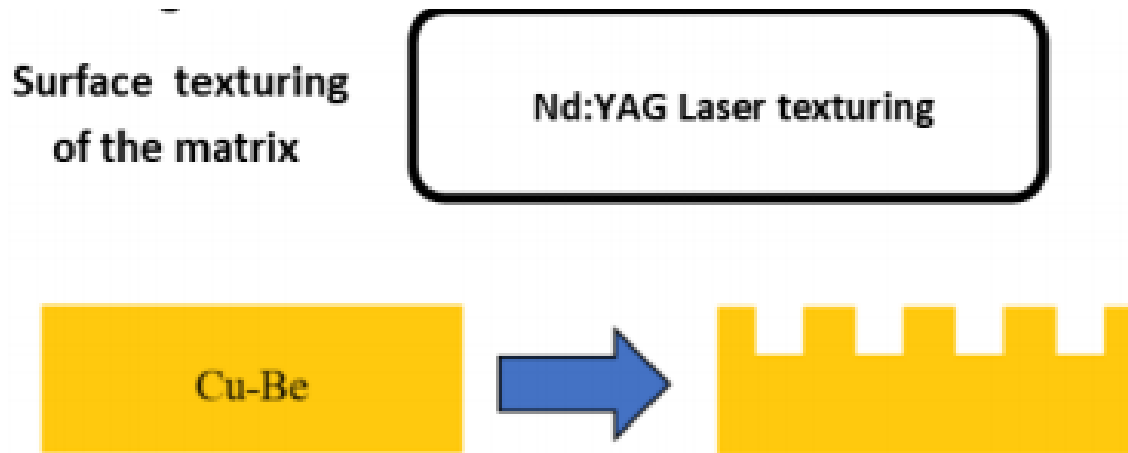


Figure.3.2. Surface texturing

### 3.1.4. Incorporation and Consolidations of functionalized diamond particles into the matrix

The two prepared materials: the functionalized powder and matrix on the plate of Cu-Be-Co integrated into each other for the preparation of the sample. The Oxide and contamination removed by sandblasting and ultrasound from the pattern/matrix surface before adding the powder to the pattern. Then the addition of functionalized diamond particles to the textured substrate was made manually by spreading a thin layer of the powder on the surface with the help of a spoon plate. To compact the powder; 250-300bar pressure applied to added powder layer on the matrix for 30minutes. Then the pre-weighted sample was fed into the electric oven for 40 minutes at 805<sup>0</sup>C, which was increased at rate 10<sup>0</sup>c/min for melting and sintering powder particles. Similarly cooled to room temperature by 10<sup>0</sup>c/min.



Figure.3.3. Reinforced matrix

The produced sample submitted to surface finishing for characterization of mechanical and tribological properties. Accordingly the surface polished;



Figure 3.4. Polished sample

### 3.2. Characterization techniques

During the different stage of sample preparation, different characterization techniques were investigated to analyze the quality of sample material as mentioned above. Additionally, the final sample investigated for the following characterization;

- ✓ The chemical composition and morphology of powder and reinforced metal matrix composite evaluation after and before pin-on-disc by 3D optical profilometry and XRD [Philips X'Pert] analyzes.
- ✓ Tribological testing: - the pin on disk tribometer used to evaluate the tribological performance of the sample for analysis of the coefficient of friction and wear track. With the following variables

Load: - 5N

Speed:-0.1m/s

Soda lime ball (SiO<sub>2</sub>, Na<sub>2</sub>O, and others), 4.56GPa of hardness

- ✓ Hardness testing: - Vickers hardness test [Karl FrankGmbh hardness machine] at a load of 1N for 15sec were used to evaluate the hardness value of samples.

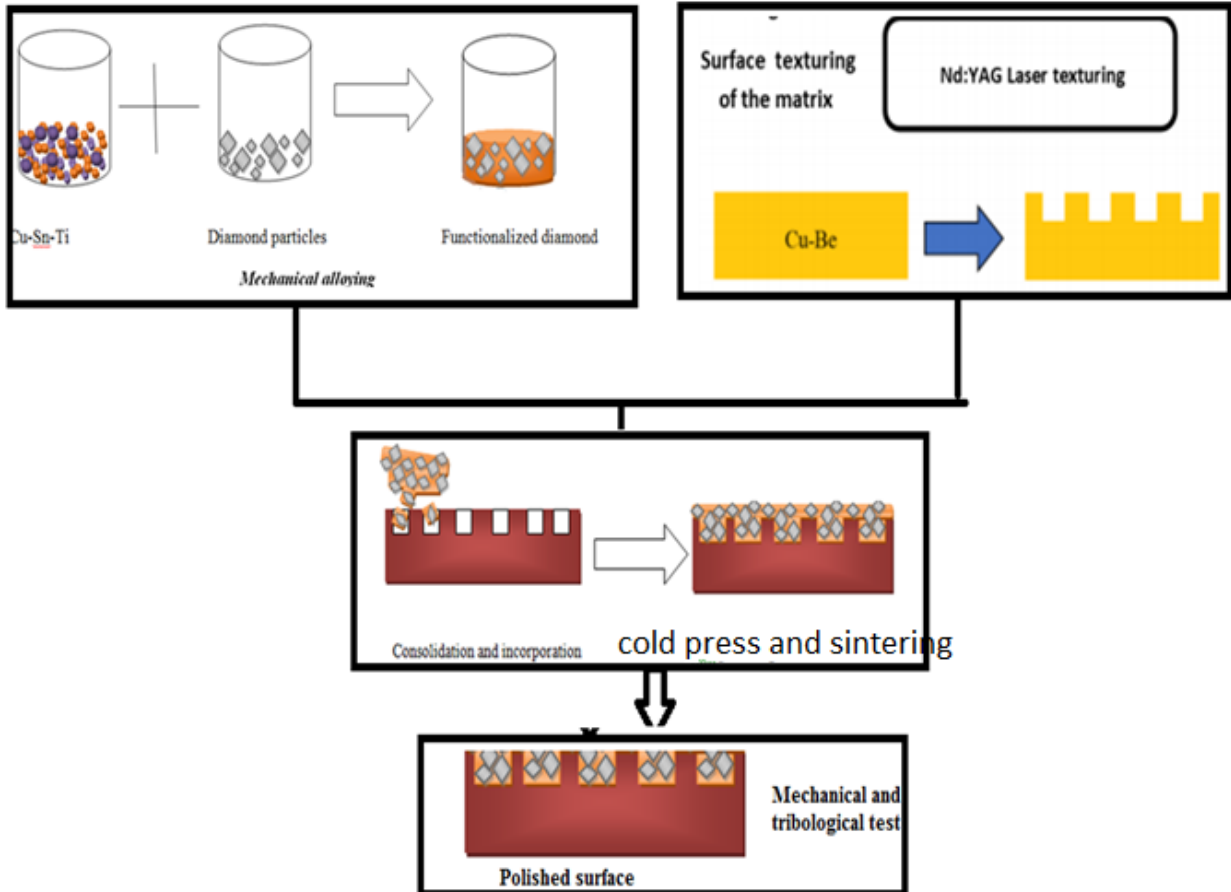


Figure .3.5. Overall schematics of representation of activities

## Chapter Four

### 4. Result and Discussion

This chapter is divided into five subchapters and is concerned with the outcomes of the experimental work designed in the previous chapter. The first subchapter deals with the influence of temperature and time on the microstructure and hardness of the Cu-Be-Co alloy. In the second subchapter, the results of the functionalization of the diamond particles with a Cu-Ti-Sn alloy by mechanical alloying are presented. The third subchapter concerns the texturing of the Cu-Be-Co substrate. The fourth subchapter deals with the reinforcement of the textured Cu-Be-Co substrate with the functionalized diamond particles by cold isostatic press and sintering. The fifth chapter concerns with the tribological characterization of the reinforced and unreinforced Cu-Be-Co alloy. The results are discussed and compared with the ones available in the literature.

#### 4.1 Effect of temperature and time on the microstructure and hardness of the Cu-Be-Co alloy

Nine samples from a Cu-1.7% Be-0.6%Co alloy were annealed at 450 °C, 550 °C, and 650 °C for 1, 10, and 25h. Figure 4.1 shows the XRD patterns of the base material (untreated sample), and heat treated samples. The structure of the base material is formed by  $\alpha$ -Cu matrix +  $\gamma''$  precipitates, in agreement with the Cu-Be phase diagram (Fig. 1 of the appendix [1]). The diffraction peaks of the  $\gamma''$  precipitates become narrow and more intense as the temperature and time of the heat treatment increase. The size of these precipitates (Fig. 2) has been calculated through Scherrer formula. The results show that the size of  $\gamma''$  precipitates increases as the temperature and the annealing time is increased as a result of the coarsening and coalescence of the precipitates [47, 48, and 49]. For the heat treatment performed at a higher temperature and longer holding times, some additional peaks can be detected in the corresponding XRD patterns. These are ascribed to  $\gamma$  or  $\gamma'$  phase [50]. There is no presence of copper oxide phases identified in the XRD patterns of the annealed samples.

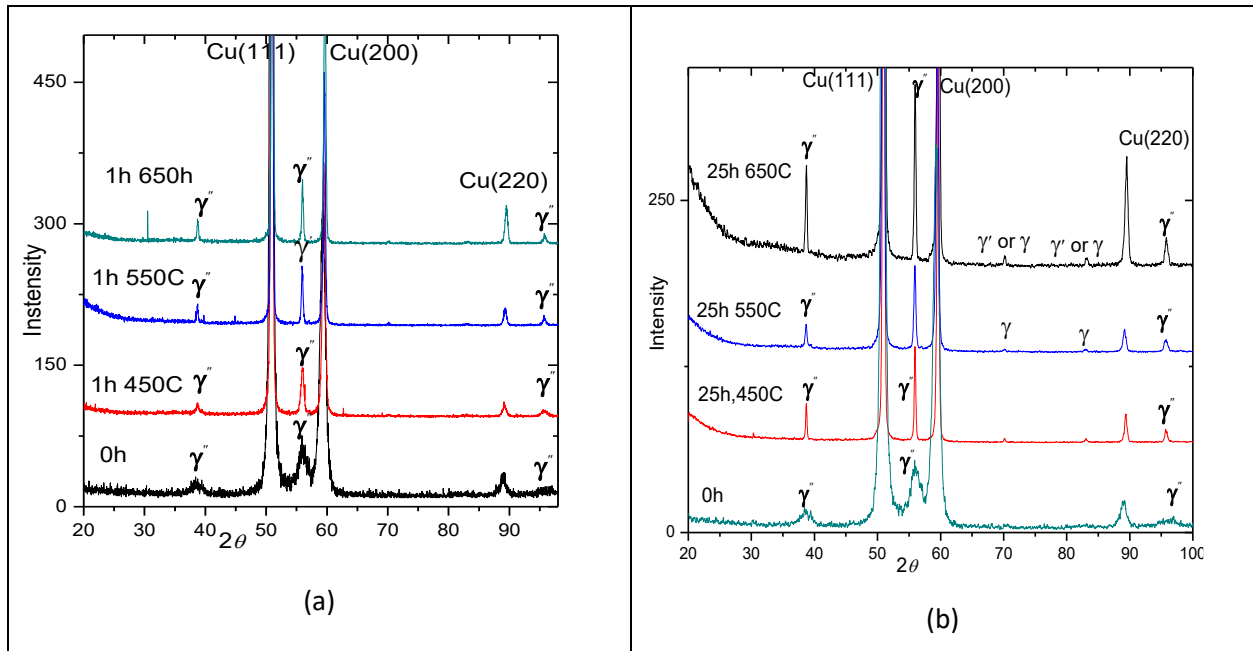


Figure 4.1 - XRD patterns of the Cu-Be-Co alloy after annealing for a) 1h and b) 25h at different temperatures

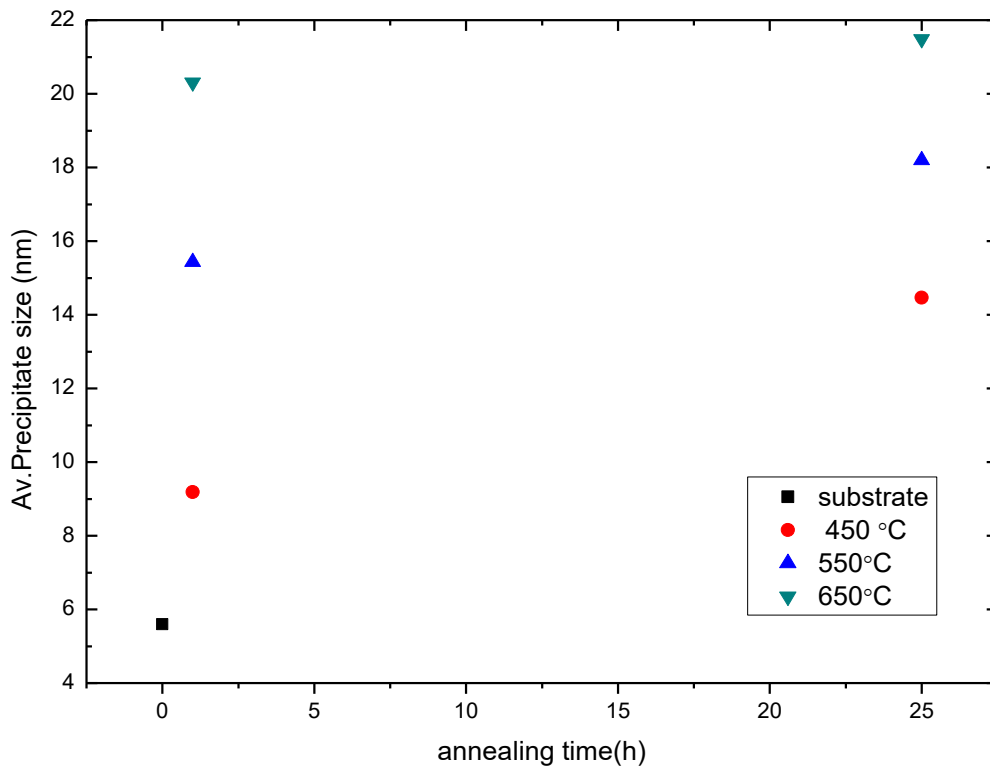
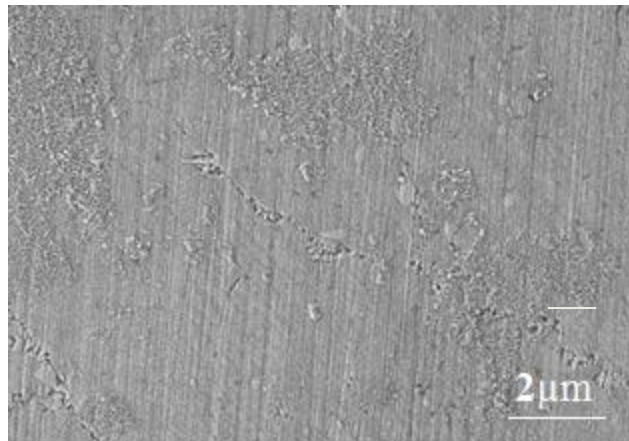


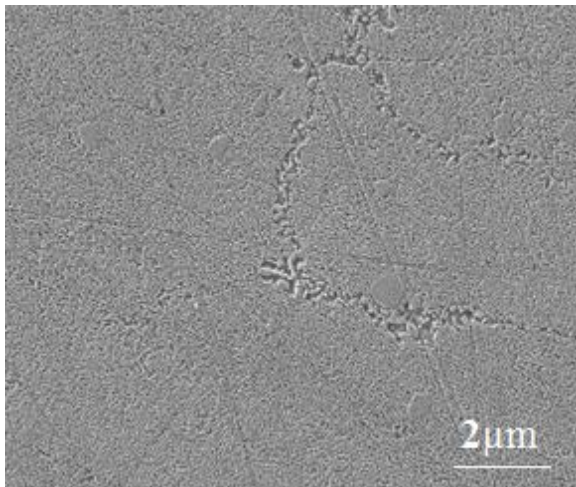
Figure 4.2. Influence of temperature and time of heat treatment on the average precipitate size

To examine further the microstructure change and precipitation behavior induced by the heat treatment of the Cu-Co-Be samples, optical microscopy, and SEM analysis was performed (figures 4.3 and 4.4). These images confirm the observations from XRD analysis and show the presence of dispersed precipitates either in the  $\alpha$ -Cu grains or in the grain boundaries. Both the temperature and time induce an increase in the size of the  $\gamma''$  precipitates. It is known that coalescence occurs by a diffusion process, which increases with increasing temperature and time, the temperature being predominant. This is the reason why the precipitates after heat treatment at 450°C / 25h and 550°C / 1h (or 550°C / 25h and 650°C / 1h) have similar sizes. After 650°C / 1h, precipitates with 2  $\mu$ m size are visible in the corresponding SEM image.

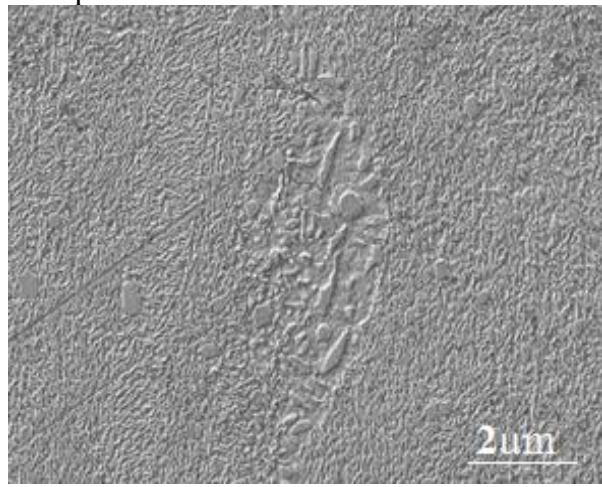
The precipitation of the  $\gamma''$  and/or  $\gamma$  phase is clearly detected by optical microscopy after annealing at high temperatures and times (figure 4.4).



Untreated sample



450 °C / 1h



450 °C / 25h

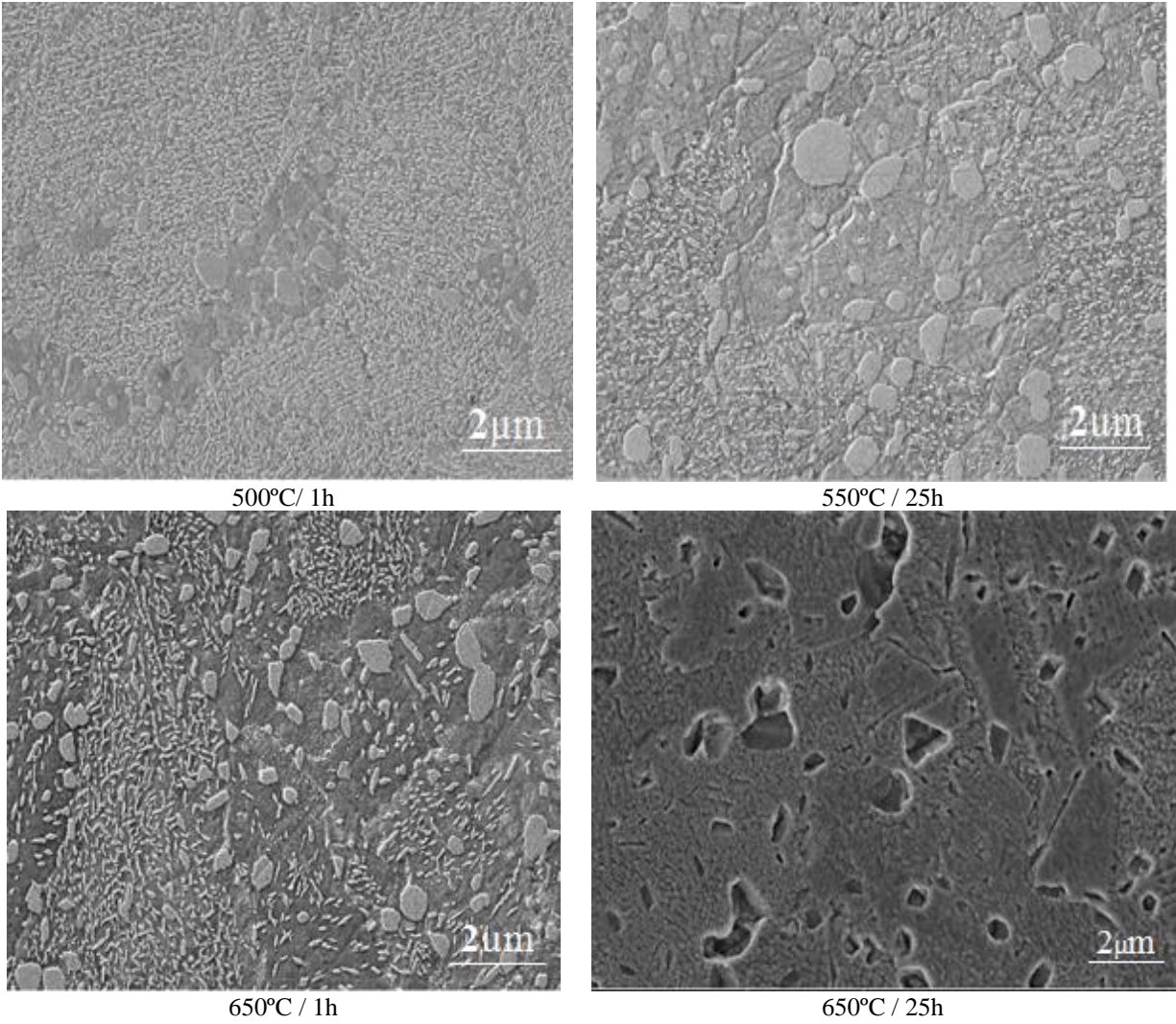


Figure.4.3. SEM micrographs of the untreated and annealed sample at different temperature and time.

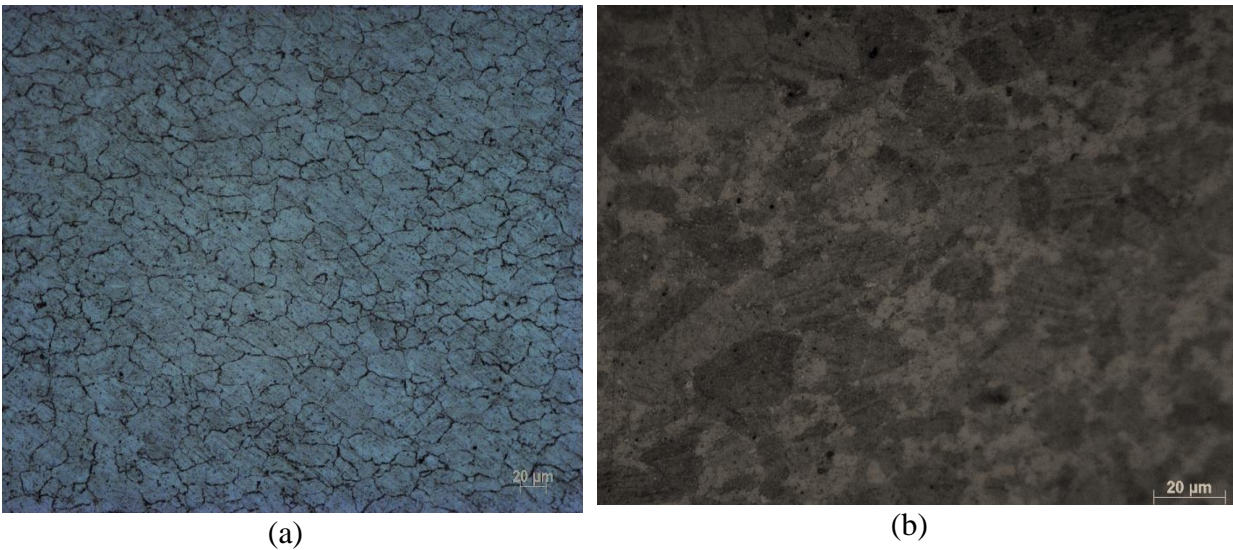


Figure 4.4 – Optical microscopy images of the untreated sample (a) and annealed sample at 550°C for 25h (b).

Figure 4.5 shows the hardness evolution as a function of the annealing time for the three studied temperatures (450, 550, and 650 °C). For a specific temperature, the hardness experiences a continuous decrease as the annealing time is increased. For instance, for 1h annealing treatment performed at 450°C and 650°C, the hardness values decrease from 2.91 to 1.6 GPa, respectively, while for 25 hours, this decrease is lower (2.4 to 1.3 GPa, respectively).

The higher the annealing temperature, and the longer the duration of the heat treatment, the lower is hardness value. This decrease is related to the dislocations mobility increase. This happens because of the dissolution of metastables  $\gamma''$  and  $\gamma'$  nano-precipitates within the copper matrix, as a result of the temperature and/or time increase [51,52].

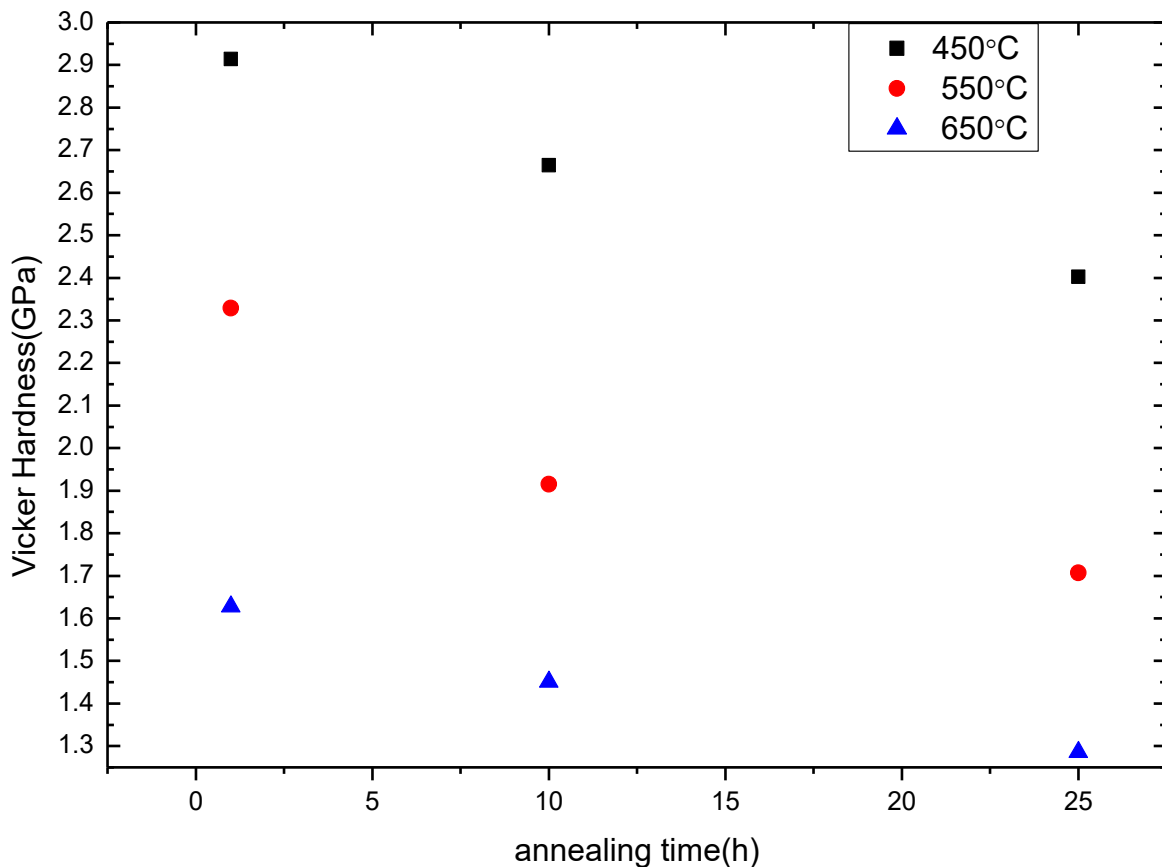


Figure.4.5. Effect of the temperature and time of the heat treatments on hardness

## 4.2. Functionalization of diamond particles

The diamond particles were functionalized with a Cu-Sn-Ti low melting alloy by mechanical alloying. The milling process was conducted at 600 rpm for 5, 10, and 25h. The evolution of the powder mixture with milling time was examined by SEM, laser scattering (Scattering Model of Fraunhofer), and XRD.

Figure 4.6 shows the evolution of the morphology of the Cu-Sn-Ti + diamond mixture with milling time. The SEM image corresponding to the initial mixture (0h) shows particles of Cu, Ti, Sn, and Diamond. After 5h milling, the Sn and Ti are no longer visible, and the diamond particles are embedded at the surface of the particles as a result of cold welding. A similar process has been reported during the functionalization of diamond particles with Ag-Cu-Ti alloy [53].

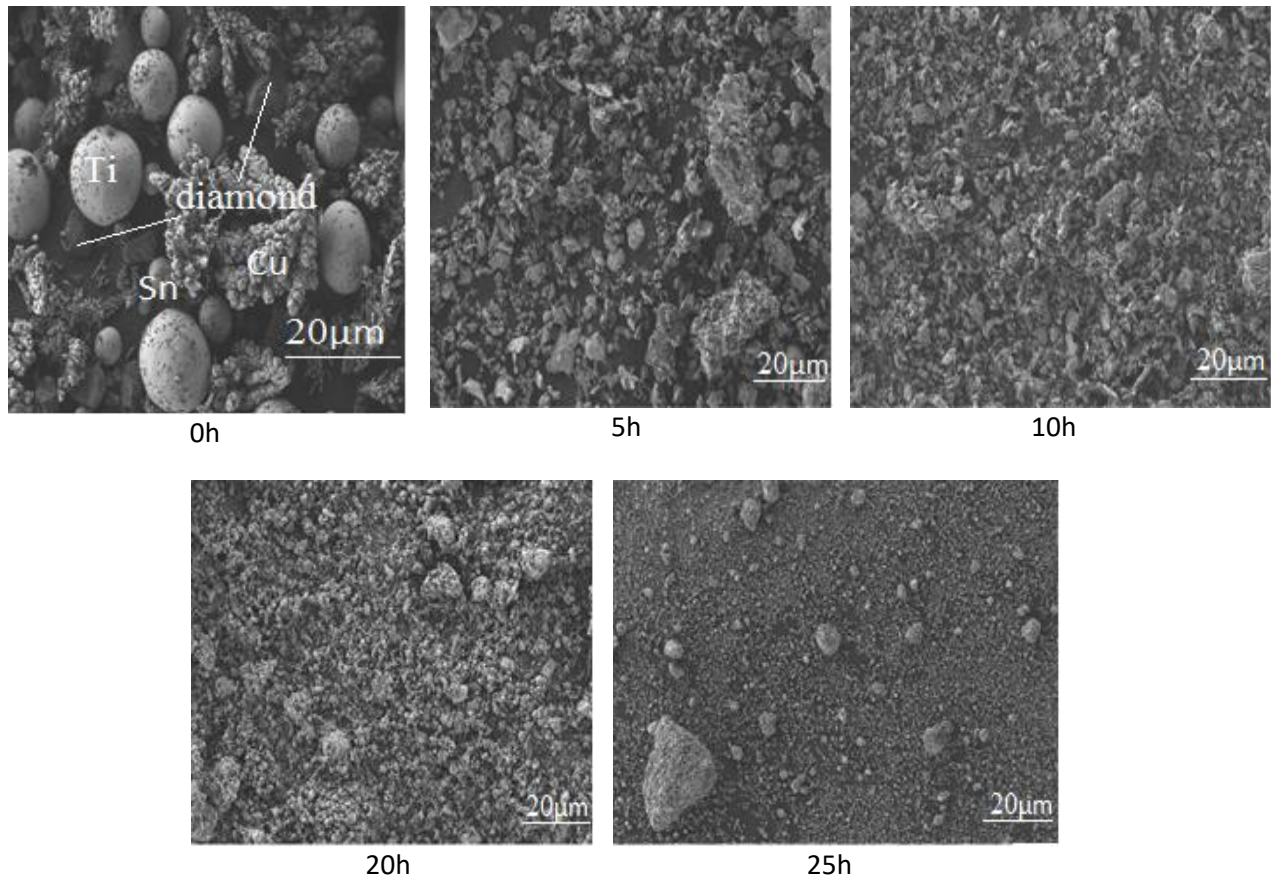


Figure.4.6.SEM micrographs of powder after mechanical alloying at 600 rpm.

Figure 4.7 shows the particle size distribution of the mixture after mechanical alloying at 600 rpm for 5h, 10h, and 25h. According to the density function, the size of the particles is in the range 0.2 – 20 $\mu\text{m}$  with a  $D_{50}$  value of 6, 3, and 3.4 $\mu\text{m}$  for 5, 10, and 25h of milling, respectively. The decreasing of  $D_{50}$ , shows breakage of particles continued during the milling process without significant change in particles size distribution as milling time increases.

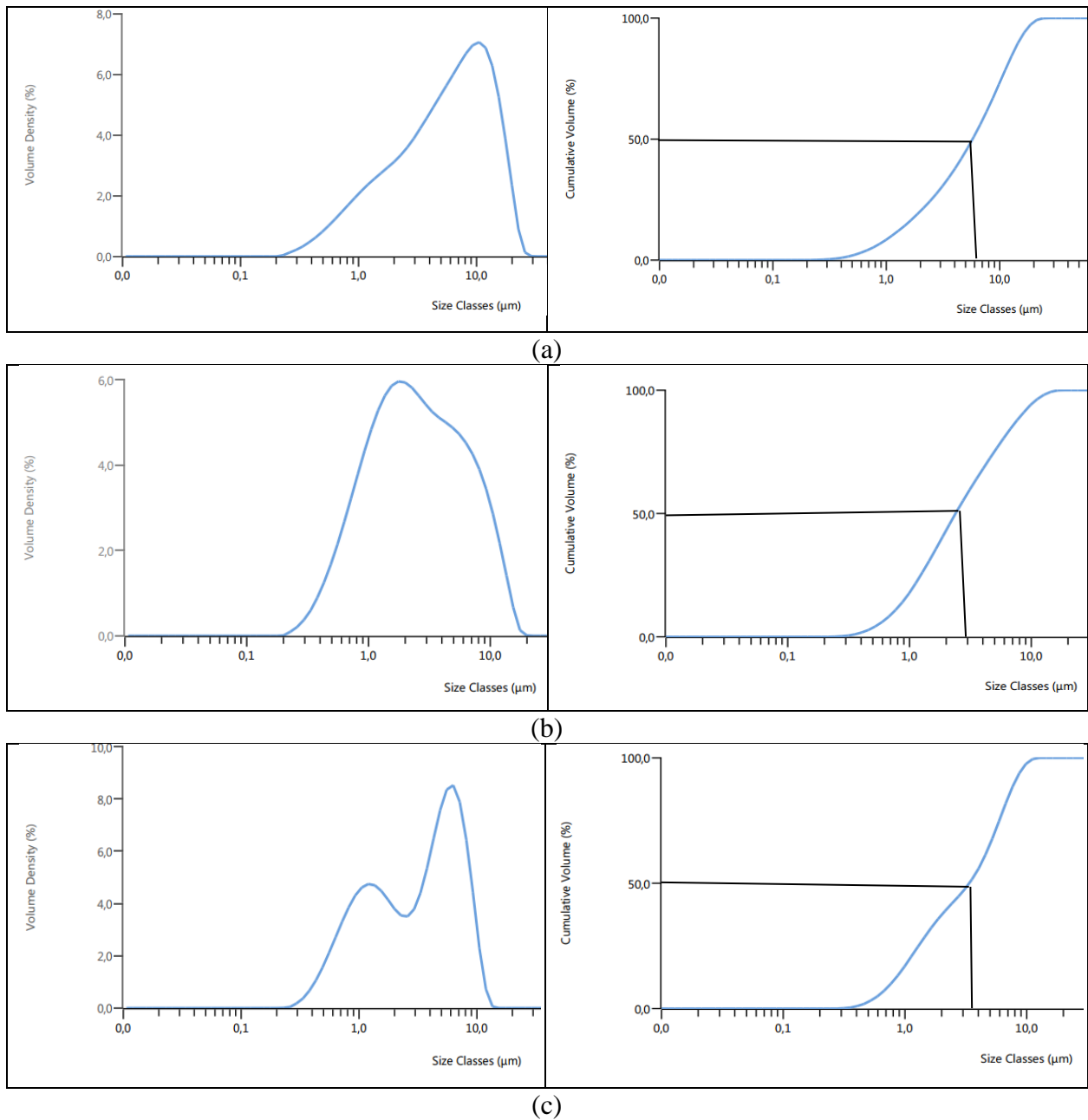


Fig. 4.7 – Particle size distribution of the mixtures after mechanical alloying at 600 rpm for (a) 5h, (b) 10h and (c) 25h.

The XRD patterns of the mechanically alloyed mixtures are shown in figure 4.8. Up to 10h milling, no structural evolution was noticed. The copper (fcc),  $\alpha$ -titanium (hcp),  $\alpha$ -tin (fcc) and diamond (fcc) are the phases present. However, for higher milling times, the XRD peaks of the titanium and tin phases are no longer visible, which can be an indication of the dissolution of these elements in the Cu phase.

In fact, there is a significant shift of the XRD peaks of this phase to lower diffraction angles with milling time. The atomic radii of titanium and tin are higher than the one of copper, 1.4, 1.45 and 1.35 Å, respectively. This means that the incorporation of titanium and tin in substitutional positions of the fcc lattice of copper leads to an increase of the unit cell parameters (Cu diffraction peaks shifted to the lower diffraction angles). The (111) peak of the diamond structure is clearly detected even 30h of milling, revealing that it stayed stable during this process. Iron contamination occurred during milling. The (110) peak of the  $\alpha$ -Fe phase, placed at  $2\theta = 52.42^\circ$  is detected mainly for the higher milling times. The presence of Sn-Ti or Cu-Ti intermetallic phases [54] were not detected even after the longest milling process.

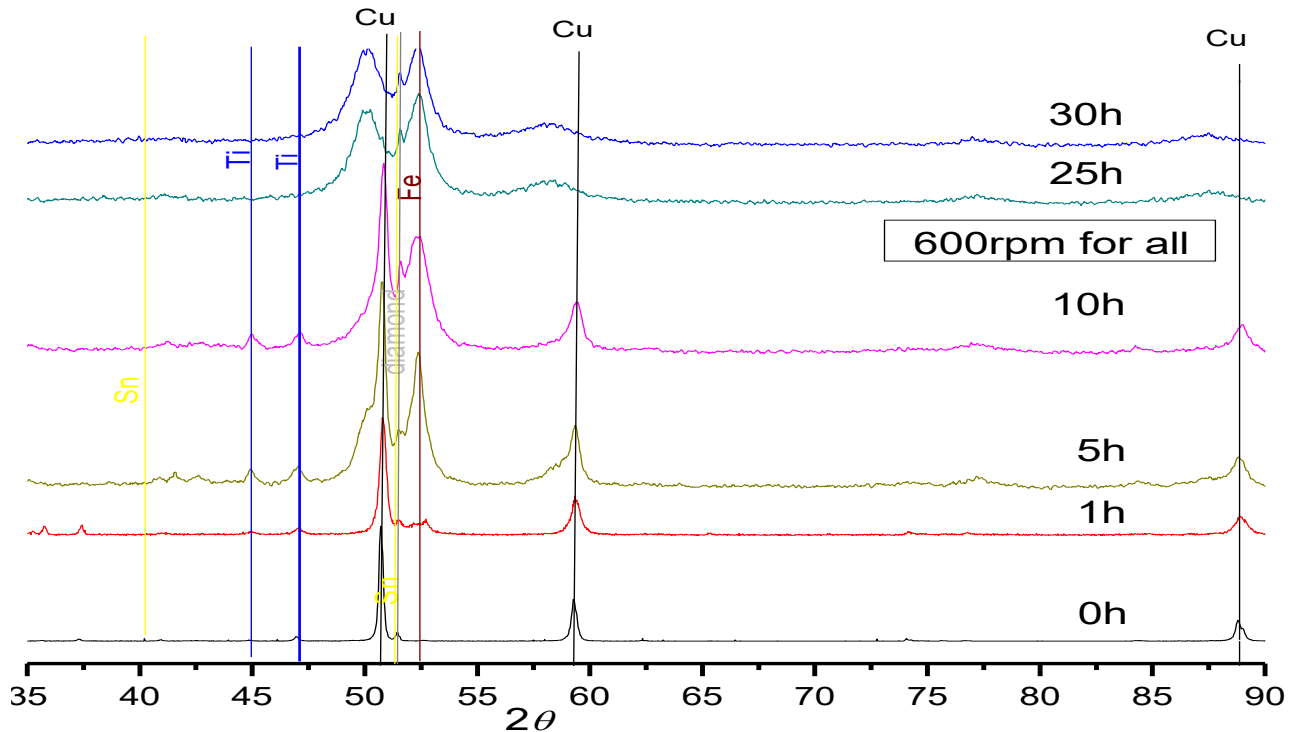
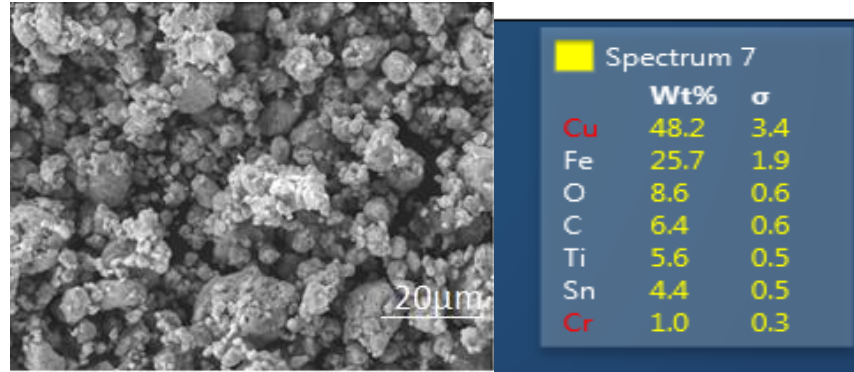
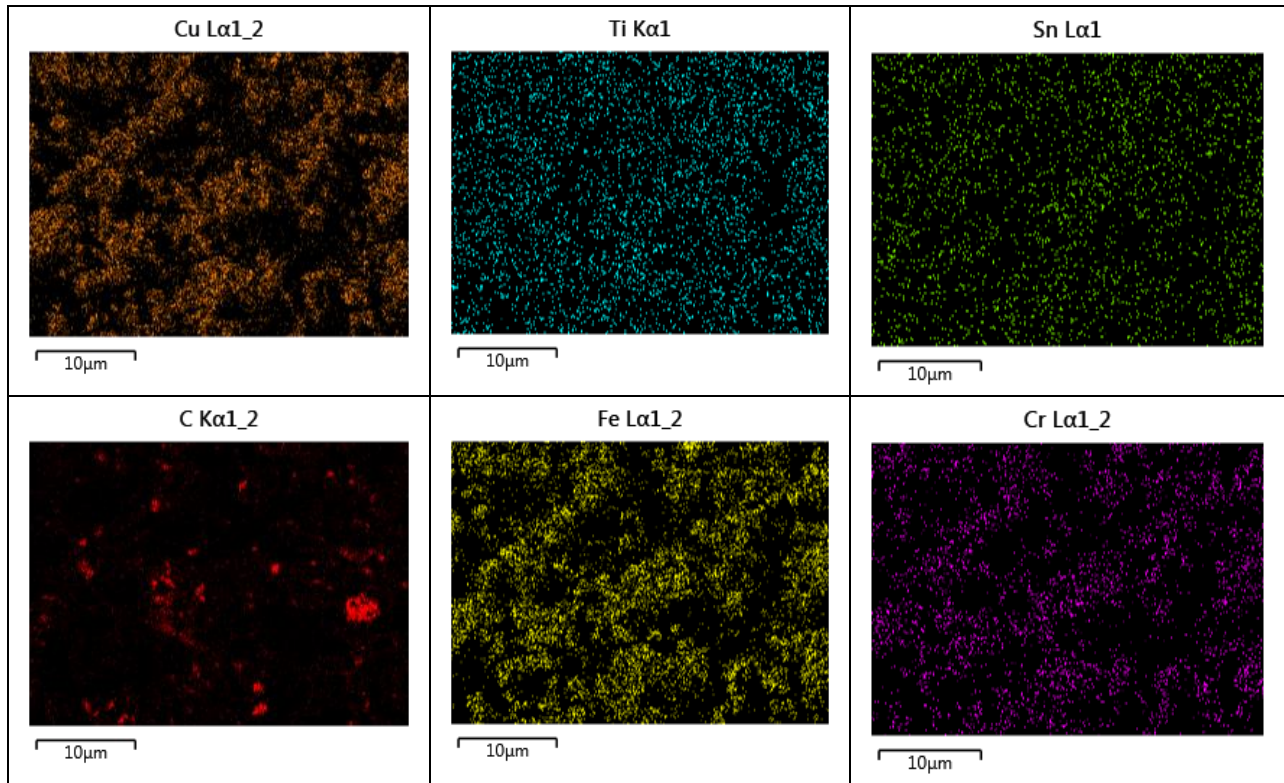


Figure.4.8. XRD diffractograms of the mixtures milled at 600 rpm for different times.

Based on the morphology, particles size distribution and XRD results, the powder milled at 25h was the one selected for further experiments. A detailed SEM micrograph and EDS results of the final powder are shown in Figure 4.9.



(a)



(b)

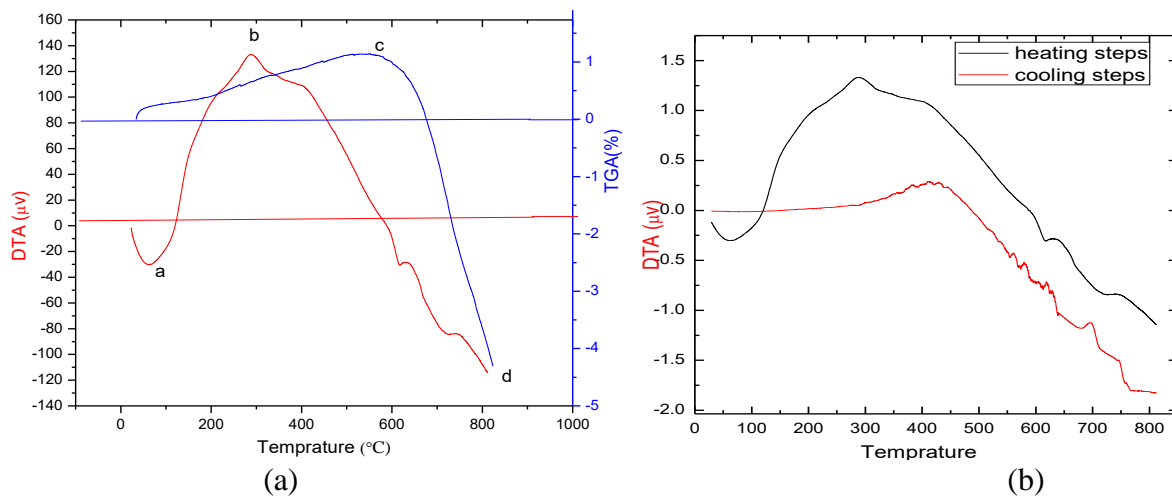
Figure.4.9. (a) SEM micrographs and (b) EDS maps distribution of powder after mechanical alloying at 600 rpm for 25

The results show homogeneous powders in terms of chemical composition and confirm the composition presented in XRD diffractograms. The distribution of the diamond particles is quite regular.

With the aim of studying the structural stability of the alloyed mixture as a function of temperature, the powder milled for 25h was submitted to TGA/DTA analysis up to 805°C (figure 4.10). After cooling down to the room temperature, the powder was analyzed by XRD (figure 4.10 e).

The TGA curve shows a progressive increase of mass up to 590°C (1.3% at this temperature) due to the oxidation of the powder (oxides of Copper, tin, and titanium ). For higher temperatures, there is a sudden reduction from 1.3 to -4% (point c to point d), this reduction is induced by phase transformation and evaporation of stearic acid [55]. The DTA curves show the following features:

- ✚ An endothermic transformation occurred from 0 to 150°C with a slight increase in mass.
- ✚ Then, an exothermic transformation happened and generated the formation of a sharp peak around 265°C with a significant increase in mass. The mass increased due to the formation of an oxide ( such as  $\text{TiO}_2$ ,  $\text{Cu}_2\text{O}$  ) during the exothermic transformation. G. Lu. et al. identified and reported the formation of oxides such as  $\text{CuO}$  or  $\text{TiO}_2$  at this temperature. [56]
- ✚ A rapid endothermic transformation with an important reduction of mass from 600°C - 800°C was observed, probably associated with the formation of new Cu-Sn phases.
- ✚ EDS/SEM and XRD analysis of the powder after the thermal cycle reveals the formation of  $\text{Ti}_2\text{O}_3$ ,  $\text{TiO}$ ,  $\text{Cu}_2\text{O}$ , and  $\text{CuO}$  oxides during the DTA run. In fact, the EDS analysis (figure 4.10(d)) confirms that oxygen is present in the final mixture in a high amount.



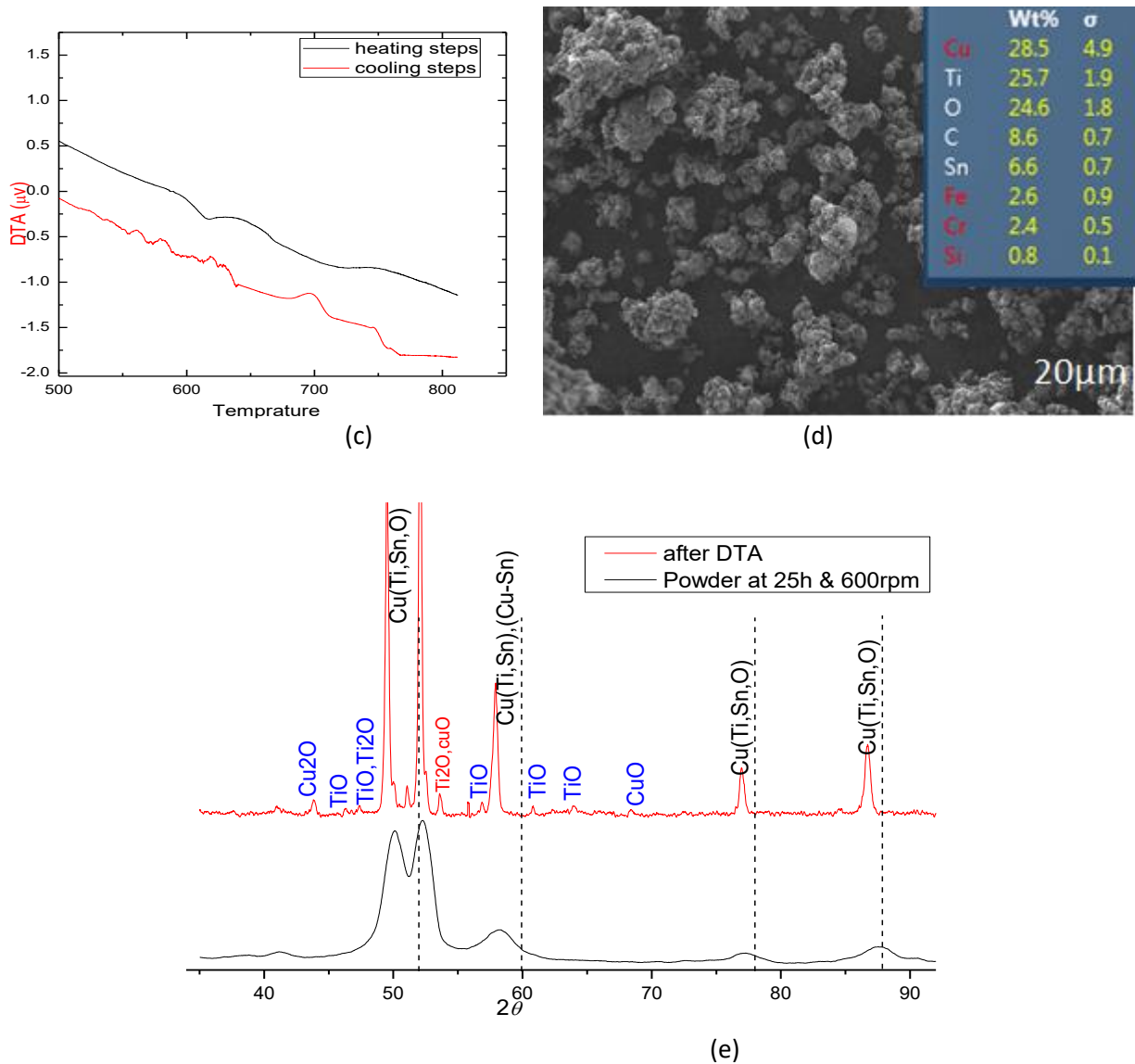


Figure.4.10. Powder milled at 600 rpm for 25h after DTA/TGA. (a) DTA/TGA graph, (b) DTA curves for cooling and heating step, (c) DTA curves for cooling and heating steps corresponds to a range of  $600^{\circ}\text{C}$ - $800^{\circ}\text{C}$ , (d) the corresponding SEM micrographs after DTA/TGA and (e) XRD pattern after DTA/TGA.

### 4.3. Texturing of the Cu-Be-Co substrate

The texture of Cu-Be-Co plates was performed by laser. Two different samples were produced with textured surface areas of 25 and 75% (distance between dimples of 60 $\mu\text{m}$  and 180 $\mu\text{m}$ , respectively). The morphology of the dimples/pattern was evaluated by optical profilometry (figure 4.11). The pattern consists of square pyramids obtained from the machining of the adjacent zones. But in terms of 75% textured sample, the upper part of dimples have a rectangular area with the irregular edge (appear as circular).

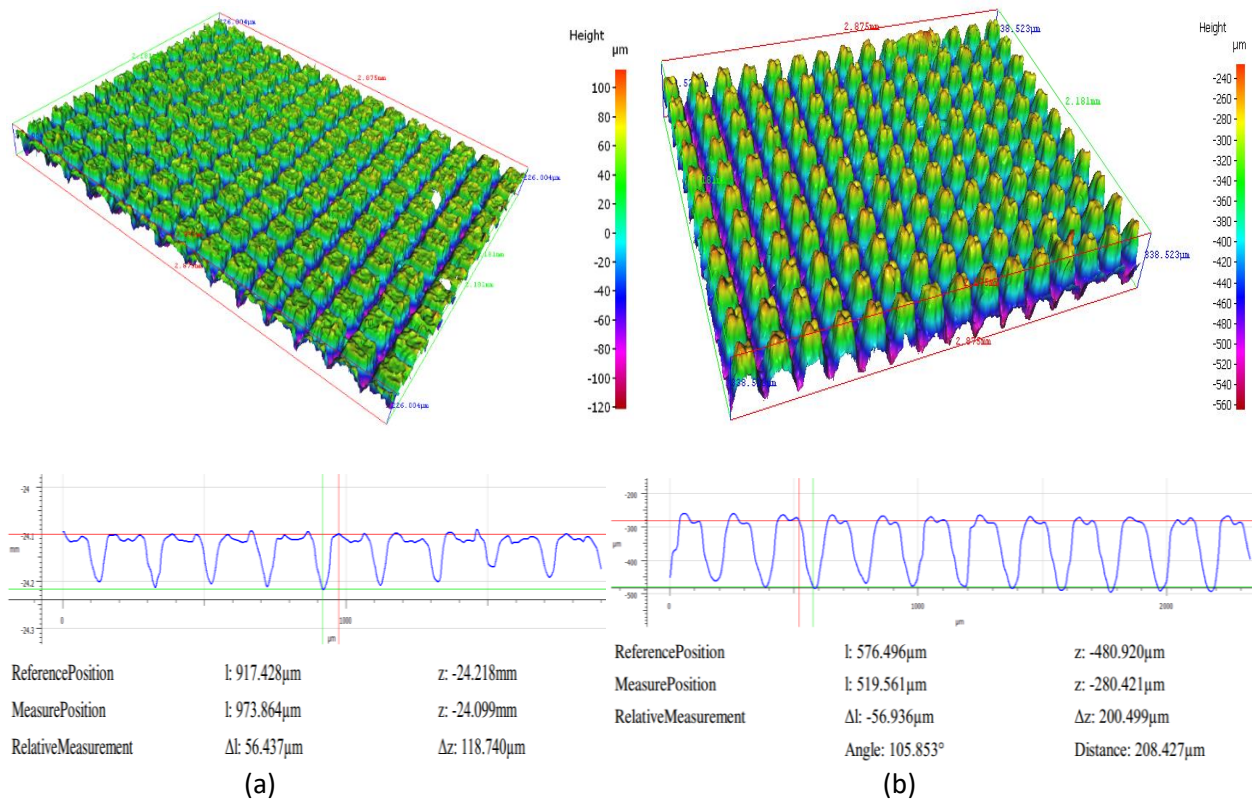


Figure 4.11 - Optical profilometry images of the Co-Be-Co textured samples. (a) 25% of the textured area and (b) 75% of the textured area.

The depth of the patterns was 118  $\mu\text{m}$  for the sample with 25% of the textured area and 200  $\mu\text{m}$  for the one with 75% of the textured area. (figure 4.11). Both values are appropriate to accommodate and settle the reinforcement of the composite particles with dimensions in the range of 0-20  $\mu\text{m}$ , as shown in section 4.2.

Figure 4.12, shows three XRD pattern of the Cu-Be-Co and textured Cu-Be-Co( $2\theta=20^\circ$  pattern XRD and low incidence degree XRD pattern ) samples. Low incidence degree of XRD pattern collected to focus on the evolution from the textured area. The diffractograms collected from the textured samples show the formation of copper oxide  $\text{CuO}_2$ , which might be explained by the fact that the samples were exposed to air during the laser texturing process.

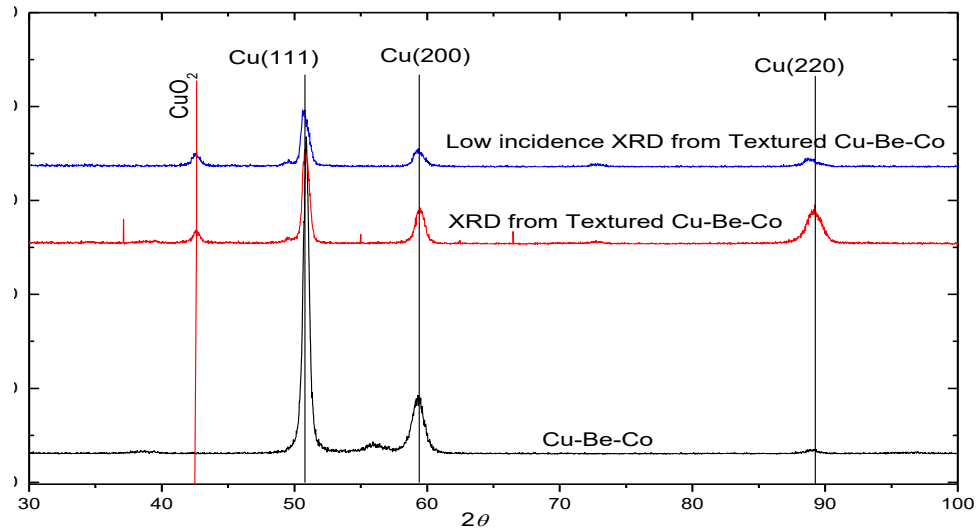


Figure 4. 12. XRD diffractograms of Cu-Be-Co substrate and Textures Cu-Be-Co( as low incidence and  $20^\circ$  XRD pattern substrate)

Table 4.1. Shows the hardness values corresponding to different zones of the textured samples. Slightly lower hardness values were obtained in the peak and valley parts of the pattern/dimples when compared to Cu-Be substrate. This happened due to the heat effect generated during laser surface texturing, as a consequence of precipitation size increases ( as discussed in section 4.1).

Table 4.1. Hardness value at 0.025 N

Type of material	Cu-Be substrate	Peak of textured Cu-Be	Valley of textured Cu-Be
Hardness Value	$3.72 \pm 0.03$	$3.69 \pm 0.12$ GPa	$3.60 \pm 0.11$ GPa
	GPa		

#### 4.4. Consolidation of the functionalized diamond powder

As described in section 3.1.2, the functionalized powder was incorporated and consolidated into the metal matrix (Cu-Be-Co) by the cold press and followed by sintering at 805°C. During consolidation, the Cu-Sn-Ti particles were melted and distributed uniformly into the dimples (Figure 4.13).

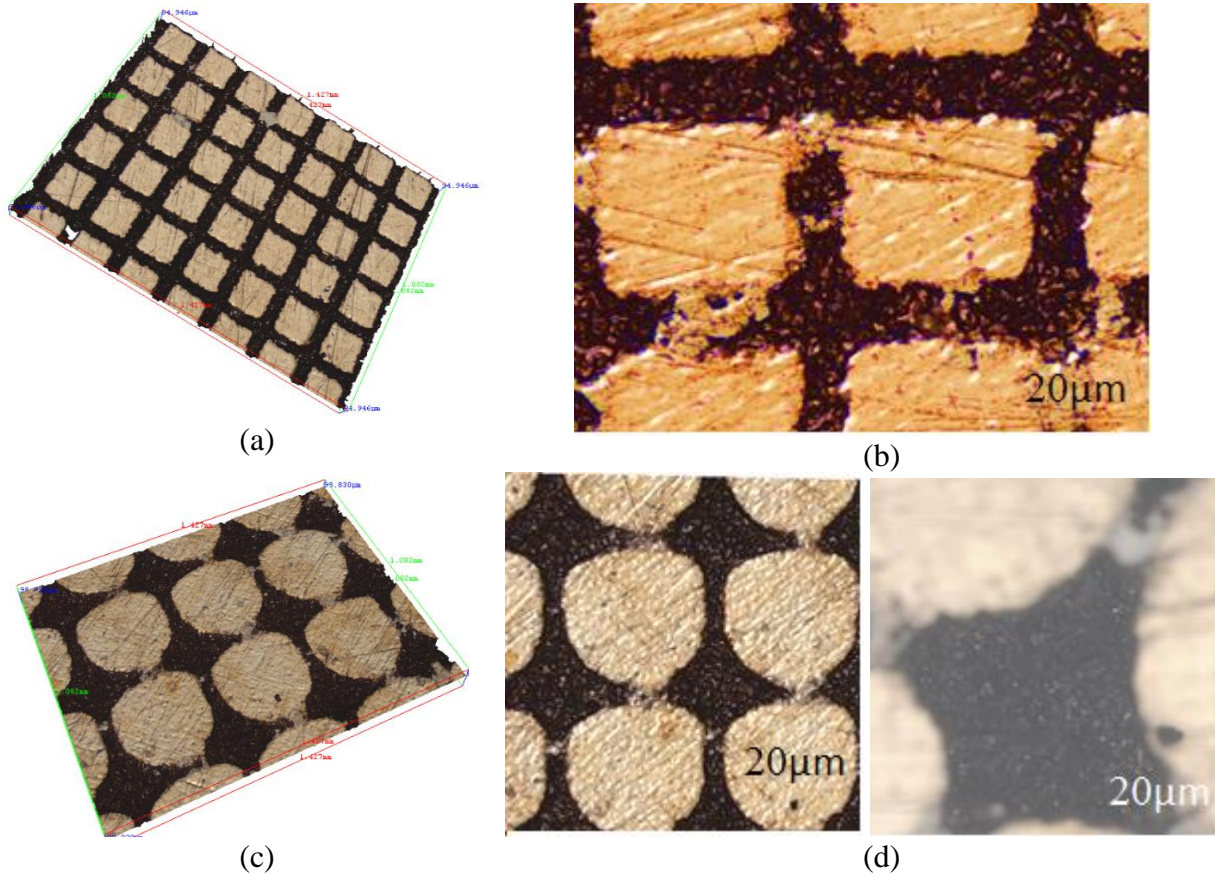


Figure 4.13. 3D and optical images of MMC,(a), 25% reinforced Sample. (b).25% reinforced samples , (c),75% Reinforced Sample ,(d), 75% Reinforced Sample .

The 25% and 75% reinforced samples have very uniform morphologies with no visible unoccupied spaces. Moreover, the interfaces between the filler powder and the substrates are quite good. These observations reveal that the consolidation/sintering process was appropriate.

Figure 4.14 shows the XRD pattern of the reinforced sample corresponds to 25%. It shows the presence of copper, diamond, and oxides phases (such as  $\text{TiO}_2$ ,  $\text{CuO}$ , and  $\text{TiO}$ ).

The hardness of the reinforced samples was evaluated by macrohardness tests. The results are presented in figure 4.15. The average hardness value of the reinforced samples suffered a decrease when compared to the untextured sample (1.61 GPa for the bare Cu-Be-Co alloy submitted to heat treatments at 805<sup>0</sup>C and 0.70-0.75 GPa for the textured samples). This can be explained by the relative hardness values and volume percentage of the constituents of the composite introduced. Although the diamond is extremely hard [57], the higher volumetric proportion of the composite refers to the Cu-Ti-Sn eutectic alloy that has low hardness.

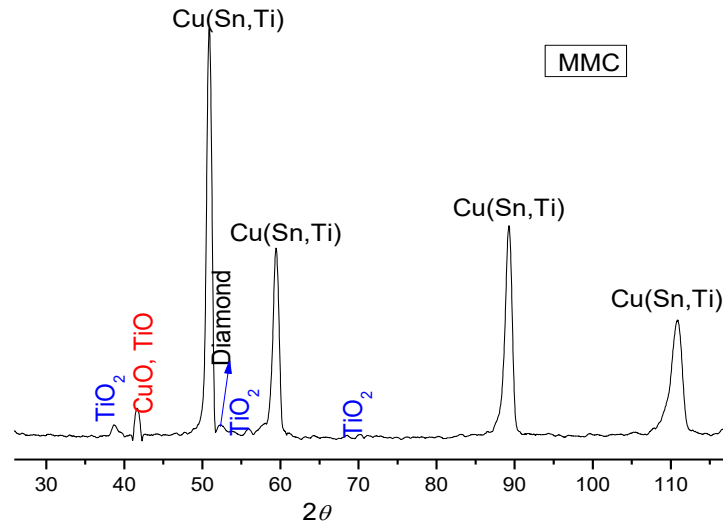


Figure 4.14 Diffractogram of the reinforced sample corresponds to 25%.

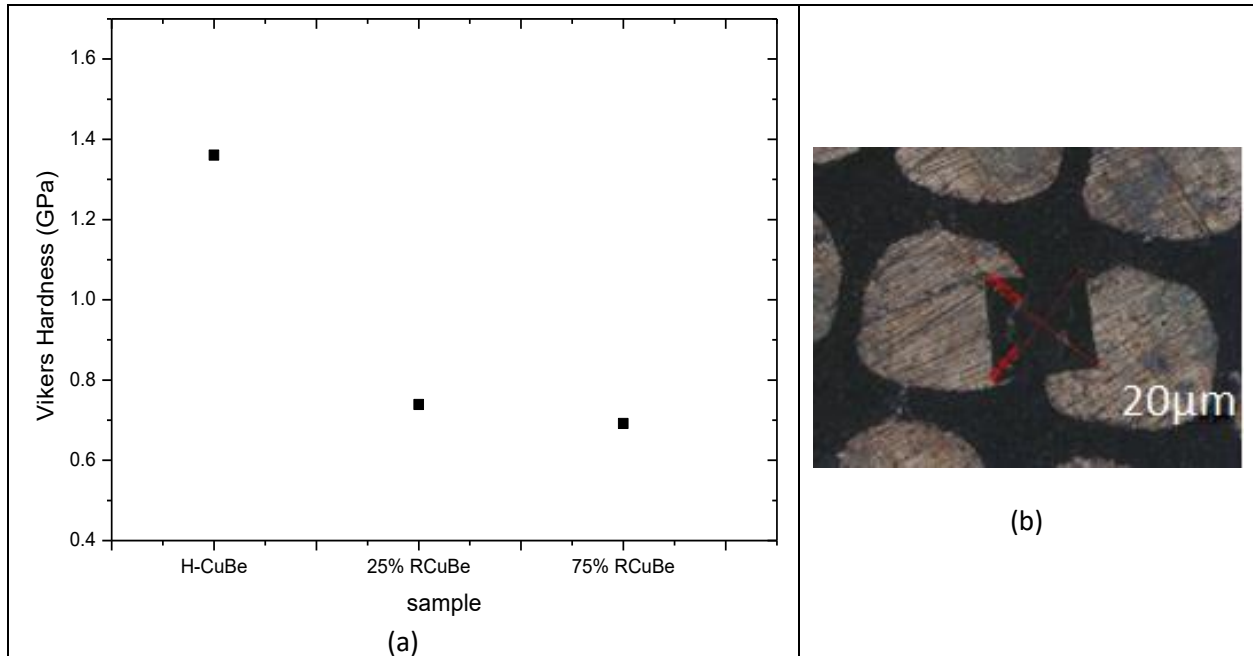


Figure 4.15: (a) Vickers hardness (5N) of bare Cu-Be and the MMC. (b) Image of one of the indentations made on the R-Cu-Be.

#### 4.5. Tribological testing

The COFs of the reinforced Cu-Be-Co and unreinforced (initial state and sample submitted to 805<sup>o</sup>C for 40min (designated as Heated Cu-Be-Co)) samples against the glass balls were recorded during the wear tests (Fig. 4.16). The evolution of the coefficient of friction (COF) with the sliding distance was characterized by two regimes: (i) running-in regime, where a significant change of the COF was observed, since the nominal contact between ball and specimen was not yet adjusted, and (ii) steady-state regime where the COF value showed small oscillations but remained approximately constant till the end of the test.

The COF values presented in this study correspond to the steady-state regime. Comparing the various COF curves, it can be concluded that reduced values were obtained for the reinforced samples when compared to the unreinforced one. Values of 0.57 and 0.512 were recorded for the unreinforced and 75% reinforced samples, respectively, corresponding to an 11% decrease. The higher the percentage of the reinforcement the lower the coefficient of friction.

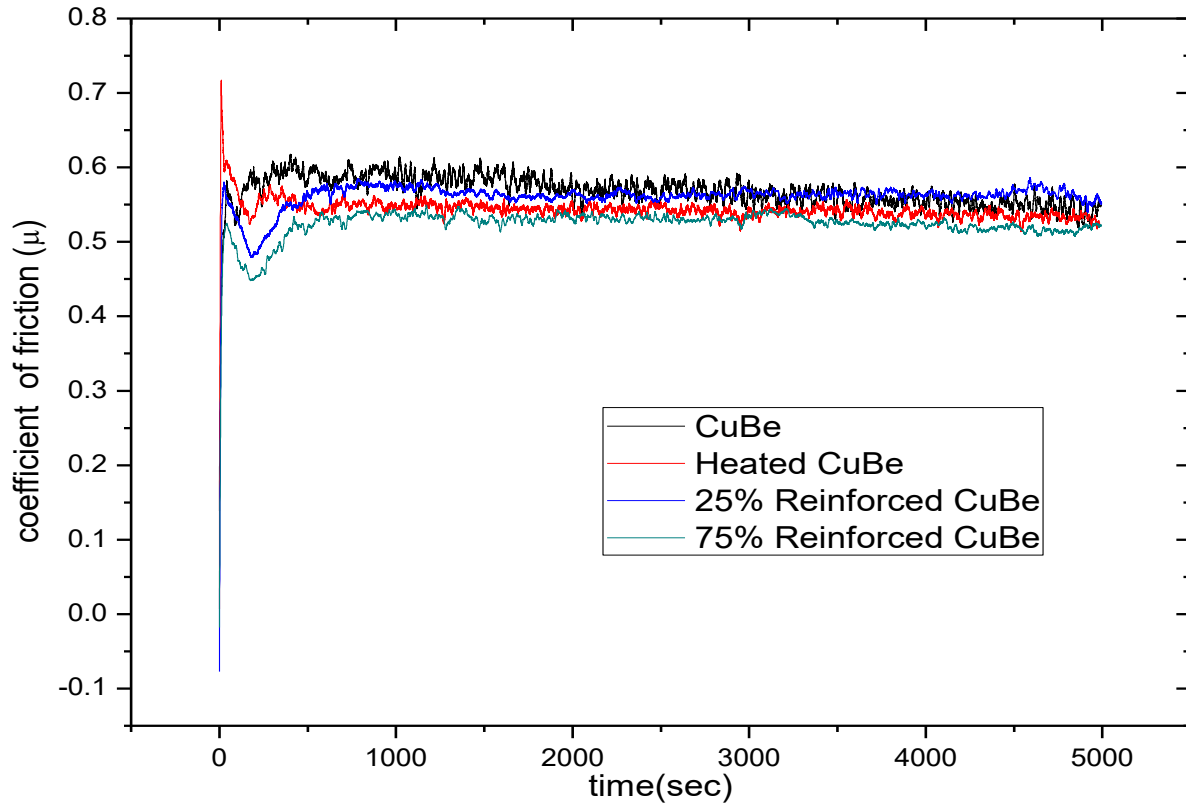


Figure 4.16: COF during the tribological tests of unreinforced Cu-Be-Co (initial state and submitted to heat treatments and R-Cu-Be-Co).

The wear track profiles were evaluated by 3D optical microscopy (Fig. 4.17). The observation of the worn surfaces revealed, especially for the unreinforced Cu-Be-Co substrate, high affected zones by wear. The abrasive wear and the depth of wear tracks decreased significantly, as the reinforcement of functionalized diamond particles increases to 25% and 75%.

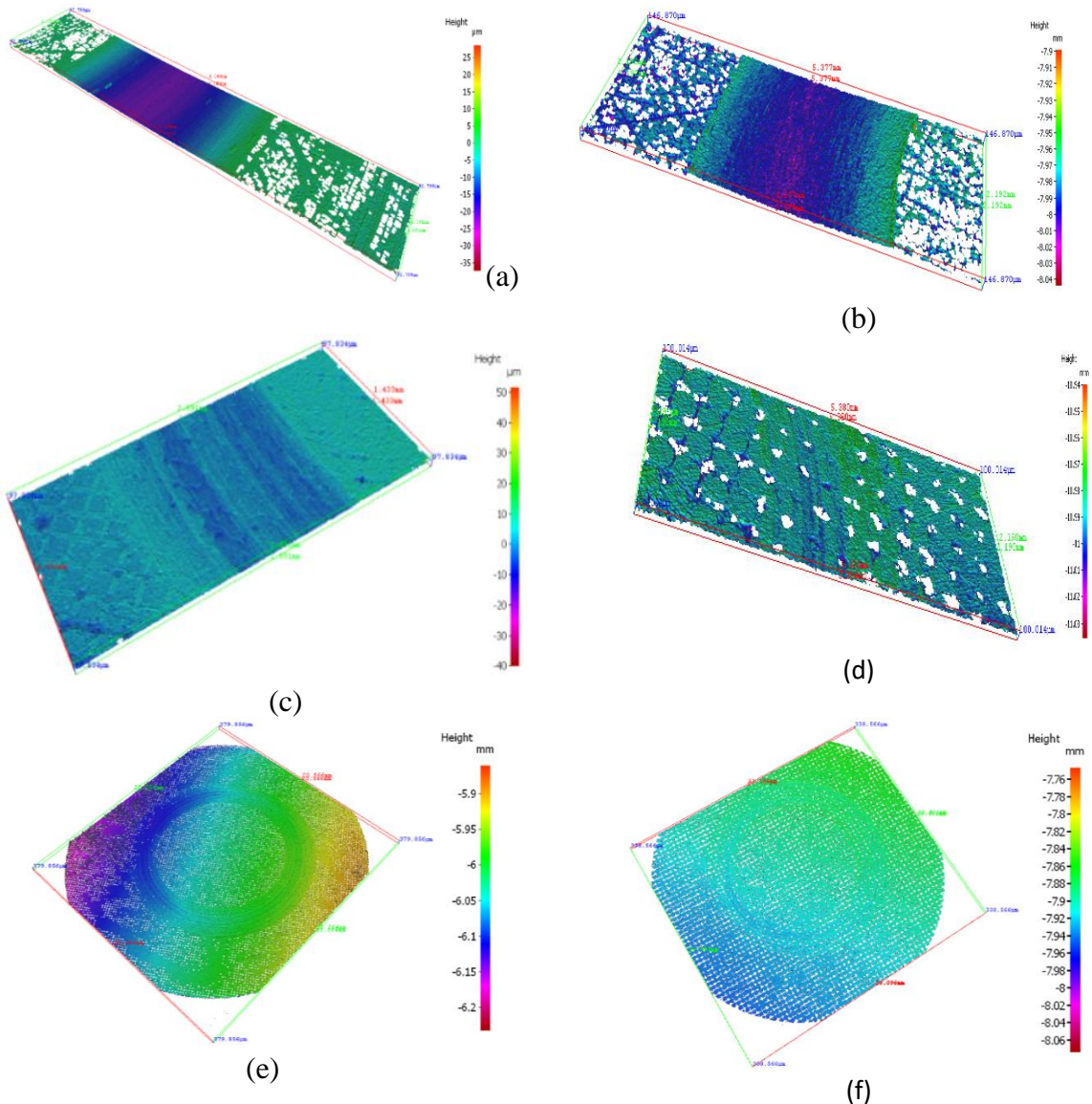


Figure 4.17. Sections were taken by 3D profilometer from the wear track corresponding with the samples: a) bare CuBe surface without annealing treatment, b) bare CuBe surface after annealing treatment, c) CuBe surface with a 25% of reinforcement and d) CuBe surface with a 75% of reinforcement. e) Full wear track of CuBe surface with 25% of reinforcement, f) Full wear track of CuBe surface with 75% of reinforcement.

Figure 4.18 presents the wear track images, which show parallel traces on wear track, without significant distortion of surface morphology and presences of few pores after the test. Significant fracture of functionalized diamond particles was not observed on the wear track. These indicate there is a strong interfacial bond between matrix and melted functionalized particles, as well as between melted particles itself.

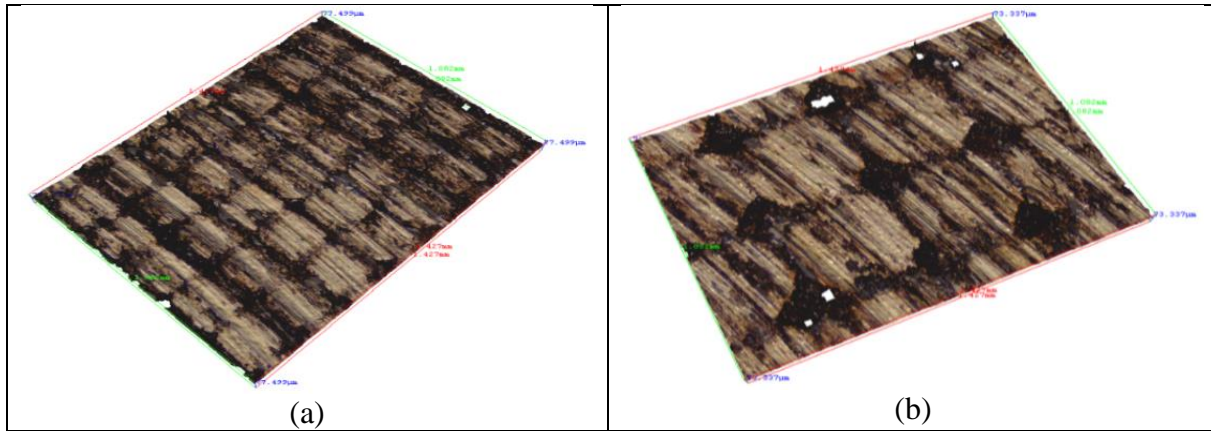


Figure 4.18. Wear track images from (a).25% and (b).75% reinforced samples.

The transversal wear track profiles can be observed in figure 4.19. As can be seen, significantly lower wear tracks depths were formed on the reinforced samples. The profile of the 75% reinforced Cu-Be-Co sample is almost flat.

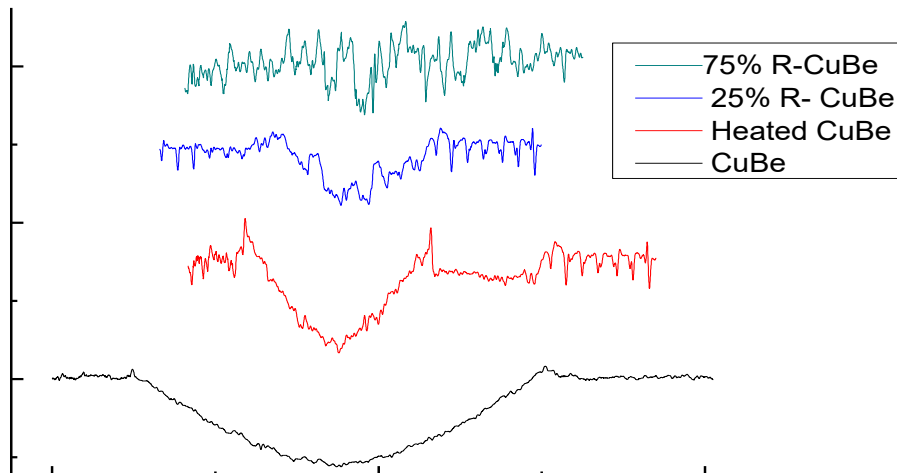


Figure 4.19: Profiles of the bare and reinforced Cu-Be after tribological testing.

The volume loss during tribological tests was calculated from the wear track profiles (appendix 2). As it can be observed in figure 4.20 and table 4.2, and as expected, the volume loss of the samples decreases, as the reinforcement percentage increases. The reduction of the wear coefficient confirms the decrease of volume loss during pin on disk tests.

The increase in the percentage of the reinforced area produces a clear effect on the counter body (glass balls Soda lime). The affected area on the balls, and their volume lost increased as the percentage of the sample filled with reinforcement increased. This is due to the presence of abrasive hard particles (diamond particles).

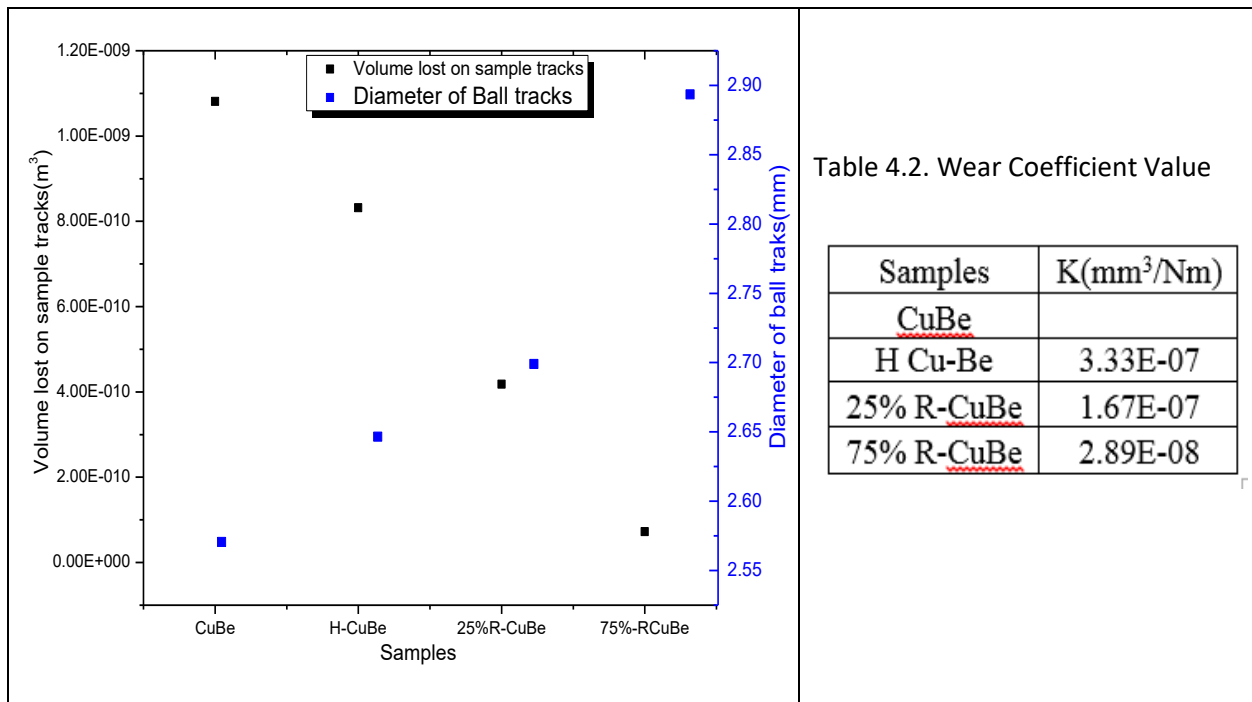


Table 4.2. Wear Coefficient Value

Samples	K(mm <sup>3</sup> /Nm)
CuBe	
H Cu-Be	3.33E-07
25% R-CuBe	1.67E-07
75% R-CuBe	2.89E-08

Figure 4.20: Diameter of the circular track on Soda lime ball and volume loss on wear track of samples due to the tribological testing.

After the tribological tests, XRD analysis was performed on the worn surfaces of the unreinforced, and 25% reinforced samples (Fig. 4.21). Oxides of TiO<sub>2</sub>, CuO, SnO<sub>2</sub>, and Cu<sub>2</sub>O were detected in the reinforced sample after tribological testing. Only the Cu-oxides was detected for the tested reinforced sample. The formation of oxides during the tribological test is responsible for the reduction of friction and wear mechanisms [58]. Diamond also plays a vital role in the friction process. The abrasive behavior of the diamond reinforced samples is dictated mainly by the presence of protruded hard diamond particles, which protect the matrix from the abrasive action of the glass balls.

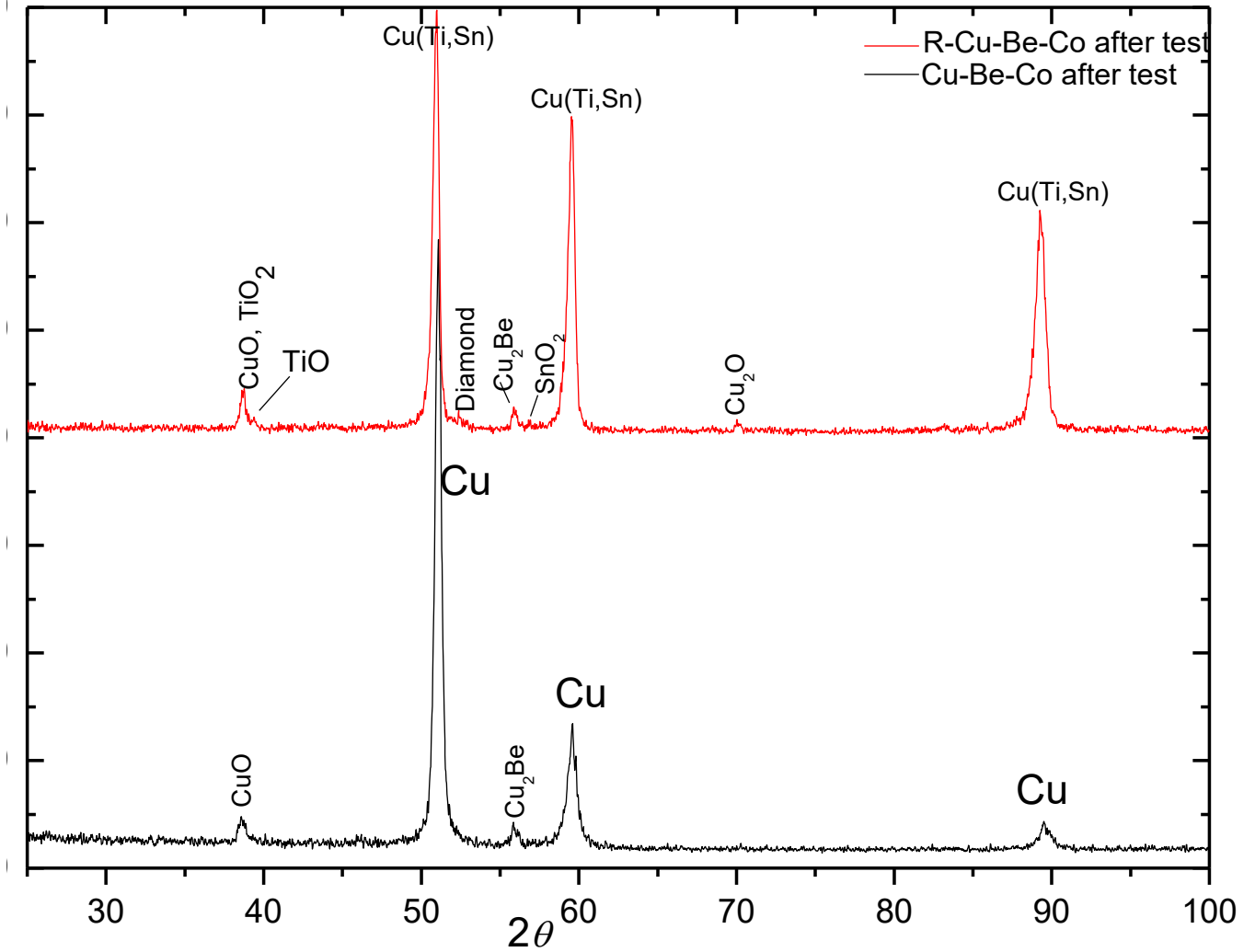


Figure 4.21. XRD diffractograms of unreinforced Cu-Be-Co after pin-on-disc and 25% Reinforced -Cu-Be-Co after pin-on-disc

## Chapter five

### 5. Conclusion

In this work, a composite blend of a low melting alloy (Cu-10Sn-15Ti) and synthetic diamond with different particle sizes were obtained by mechanical alloying and were used as a reinforcement of a laser textured CuBeCo alloy. Consolidation/sintering of the powders was conducted by cold pressing followed by sintering at 805°C.

The effect of temperature and time on the microstructure and hardness of the Cu-Be-Co alloy was studied, and the results showed that the size of  $\gamma''$  precipitates increased as the temperature and the annealing time increased, as a result of the coarsening and coalescence of the precipitates. For the heat treatment performed at the higher temperature and longer holding times, some additional XRD peaks ascribed to  $\gamma$  or  $\gamma'$  phase could be detected. The hardness experienced a continuous decrease with increasing of the annealing temperature and time.

Mechanical alloying was used to produce the composite blend of Cu-10Sn-15Ti and synthetic diamond. After 5h milling, the XRD peaks of the Sn and Ti phases were no longer visible and the diamond particles were embedded at the surface of the particles as a result of cold welding. After mechanical alloying, a homogeneous mixture of a Cu solid solution, with titanium and tin, and embedded diamond particles was obtained. The size of the particles after mechanical alloying were in the range 0.2 – 20  $\mu\text{m}$  with a  $D_{50}$  value of 3.4  $\mu\text{m}$  for 25h of milling.

The texture of Cu-Be-Co plates was achieved by laser. Two different samples were produced with textured surface areas of 25 and 75%. The patterns consisted of square pyramids obtained from the machining of the adjacent zones, with depths of 100 and 200  $\mu\text{m}$ , respectively.

The mechanically alloyed mixture was incorporated in the texture by uniaxial cold pressing followed by sintering at 800°C. During sintering, the Cu-10Sn-15Ti particles were melted and were distributed uniformly into the dimples. The interfaces between the filler powder and the substrates were quite good, meaning that the consolidation / sintering process was appropriate.

The average hardness value of the reinforced samples suffered a decrease when compared to the untextured sample (1.61 Pa for the bare Cu-Be-Co alloy and 0.70-0.75 GPa for the textured samples).

The evolution of the coefficient of friction (COF) with the sliding distance characterized for reinforced and unreinforced samples. Reduced values were obtained for the reinforced samples when compared to the unreinforced one. Values of 0.57 and 0.512 were recorded for the unreinforced, and 75% reinforced samples, respectively, corresponding to an 11% decrease. The higher the percentage of the reinforcement, the lower was the coefficient of friction.

The wear rate of the 75% reinforced sample resulted approximately 12 times lower than that of the reference.

## Bibliography

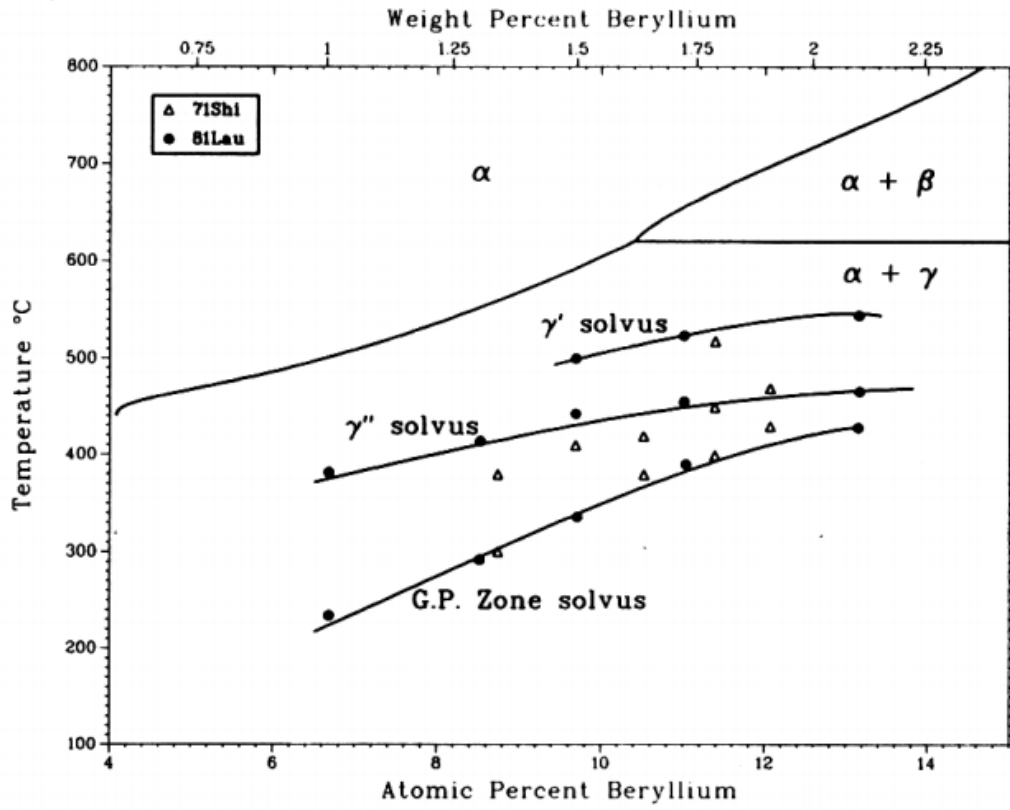
1. M. Kovac̆ec, A. Pilipovic, 2010, Improving the quality of glass containers production with plunger process control., *CIRP Journal of Manufacturing Science and Technology*. 3(2010) pp. 304-310.
2. Le. Bourhis, E. 2008, Glass: Mechanics and Technology, *Wiley-VCH, Weinheim*, ISBN: 978-3-527-31549-9, pp. 1-9.
3. Plunger for use in manufacturing glass containers, *journal of European patent* No.12/82, 2013.
4. H. P. E. Ltd., Glasstec 2016 - Cooling Tubes - Plungers - *Precision Engineering - Hunpreco Precision Engineering Ltd.* Jan 2014.
5. A. Warude, 2004, Analysis of glass mold to enhance rate of heat transfer. *PhD thesis*, 2004.
6. V. John , M. Charles ,2016, Metal-Matrix Composites, *ASM Handbook Committee*, DOI: 10.1361/asmhba0001101, pp. 903-912.
7. N. Chawla, K. Chawla, 2013, Metal Matrix Composites. *New York, NY: Springer New York*, jan 2013 pp 8.
8. S. Mahdavi, F. Akhlaghi, 2011, Effect of SiC content on the processing, compaction behavior, and properties of Al6061/SiC/Gr hybrid composites. *J Mater Sci* 2011;46: pp 1502–1511.
9. I .Etsion, G. Halperin. 2004, Experimental investigation of laser surface textured parallel thrust bearings. *Tribol. Lett.* 2004, 17, pp 295–300.
10. M. Kovačec, A. Pilipović, and N. Stefanić, 2010, Improving the quality of glass containers ~ production with plunger process control, *CIRP Journal of Manufacturing Science and Technology*, vol. 3, jan 2010, pp. 204–211.
11. Le. Bourhis, 2008, Glass: Mechanics and Technology, *Wiley-VCH, Weinheim*, ISBN: 978-3-527-31549-9.
12. M. Norouzi, Tribological and Mechanical Characterization of Copper alloy/diamond Composites for the Use in Glass Molding Industry. *PhD thesis*, 2017.
13. B. Wellman, “Guide to Beryllium Copper.”
14. P. Roger, 2017, Operational characteristics of the NNPB plunger in the glass container industry, *Phd dissertation, university of shiefild*, 2017.
15. “CES EduPack,” 2016.
16. J. Mortensen, C, Cornie 1988, Solidification Processing of Metal-Matrix Composites, *J. Met.*, Feb 1988, pp 12
17. N. Natarajan, V. Krishnaraj, and J. P. Davim, 2015, Metal Matrix Composites. *Cham: Springer International Publishing*, jan 2015.
18. J .Silvain, Y. Lepetitcorps , E. Sellier.,1994, Elastic Moduli, Thermal Expansion and Microstructure of Copper - Matrix Composite Reinforced by Continuous Graphite Fibres, *Composites*, Vol.25, No.7,1994 , pp.570-574,.

19. M. Haghshenas, 2015, Metal–Matrix Composites, *Materials Science and Materials Engineering*. DOI: 10.1016/B978-0-12-803581-8.03950-3.
20. Copper and copper alloys. *Materials Park, OH: ASM International*, 2001.
21. J. Sorensen., 2011. Great Potential (Still) for Metal Matrix Composite Structures, *CPS Technologies Blog*.
22. B. Wellman, “Guide to Beryllium Copper.”
23. J.Wu, Y. Zhou, J.Wang, 2006, Tribological behavior of Ti2SnC particulate reinforced copper matrix composites, *Materials Science and Engineering A* 422 (2006) .pp 266–271.
24. D. Hughes, 1988, Textron Unit Makes Reinforced Titanium, Aluminum Parts, *Aviat. Week Space Technol.*, 28 Nov 1988
25. K. Yoshida, H. Morigami. 2004, Thermal properties of diamond/copper composite materials. *Microelectron Rel* 2004; 44: pp 303–308.
26. D. Miracle, 2005, “Metal matrix composites—from science to technological significance,” *Composites Science and Technology*, vol. 65, no. 15-16, 2005. pp. 2526–2540.
27. B. Liu, J. Xie, and X. Qu, 2008, Fabrication of W-Cu functionally graded materials with high density by particle size adjustment and solid state hot press, *Composites Science and Technology*, vol. 68, no. 6, 2008 , pp. 1539–1547.
28. Ch. Chung, Ch. Chu,. Properties of Diamond/Cu-Ti Composites Fabricated, *Applied Thermal Engineering* 69(s 1–2): pp 208–213.
29. J. Wu, H. Zhang, Y. Zhang, J. Li, and X. Wang, 2012, Effect of copper content on the thermal conductivity and thermal expansion of Al-Cu/diamond composites, *Materials and Design*, vol. 39, pp. 2012’. pp. 87–92.
30. K. Yoshida, H. Morigami, Thermal properties of diamond/copper composite material, *Microelectronics Reliability*, vol. 44, no. 2, pp. 103–108.
31. Ch. Chung, Ch.Chu, M. Lee, 2014 , Effect of Titanium Addition on the Thermal Properties of Diamond/Cu-Ti Composites Fabricated by Pressureless Liquid-Phase Sintering Technique. *World scientific journals*, Volume 7, 2014, doi.org/10.1155/2014/71353. pp. 12–23.
32. Y. Sahin, K. Oksuz, 2011, Tribological behavior of diamond-reinforced Fe-Co composite by Taguchi method. *18th international conference on composite materials iccm-18*, at jeju island, south korea, 21-26 august, 2011.
33. M. Sherif, 2015, Mechanical Alloying For Fabrication Of Advanced Engineering Materials, *Handbooks*. ISBN: 0-8155-1462-X. pp. 1242–1250.
34. M. Adamiak, J. Fogagnolo, E. Ruiz-Navas, L. Dobrzański, 2006, Mechanically milled AA6061/(Ti3Al)p MMC reinforced with intermetallics - the structure and properties, *Journal of Materials Processing Technology* 145-156 (2004) 2002-2006), pp. 155.

35. S. Campbell, a W. Kaczmarek , 2011 Mössbauer Spectroscopy Applied to Materials and Magnetism, (G. J. Long and F. Grandjean, eds.) Plenum Press, New York, 2:273.
36. C. Machio, H. Chikwanda, S. Chikosha, 2011, Effect of process control agent (PCA) on the characteristics of mechanically alloyed Ti-Mg powders, *The Journal of The Southern African Institute of Mining and Metallurgy* . Vol. 111, SA ISSN 0038–223X/3.00, pp 149-153.
37. E. Kasapgil, İ .Anaç 2016, Effect of Stearic Acid Amount on the High Energy Milling Behavior of Atomized Iron Powders, *UCTEA Chamber of Metallurgical & Materials Engineers, Proceedings Book*, pp 898.
38. Ö. Balcı, K Gokuldoss . 2010, Effect of process control agent (PCA) on time, Effect of Milling Time and the Consolidation Process on the Properties of Al Matrix Composites Reinforced with Fe-Based Glassy Particles. *metals* ISSN 2075-4701, doi:10.3390/met5020669.
39. I. Etsion, 2004 ,Improving tribological performance of mechanical components by laser surface texturing. *Tribol. Lett.* 2004, 17, pp 733–737.
40. E. Willis, 1986, “Surface Finish in Relation to Cylinder Liners,” *Wear*, 109, pp. 351-366.
41. D. Gropper; L Wang. 2016. Hydrodynamic lubrication of textured surfaces: A review of modeling techniques and key findings. *Tribol. Int.* 2016, 94, pp 509–529.
42. I. Etsion, Y. Kligerman. G. Halperin, 1999, Analytical and Experimental Investigation of Laser-Textured Mechanical Seal Faces, *Tribology Trans.*, 42(3), pp. 511-516.
43. L. Hu, Q. Ding, 2012, The effect of laser surface texturing on the tribological behavior of Ti-6Al-4V, *J Engineering Tribology*, 226(10) pp 854–863.
44. J. Deng, W. Song, H. Zhang, P. Yan, A. Liu, 2011, Friction and wear behaviors of the carbide tools embedded with solid lubricants in sliding wear tests and in dry cutting processes, *Wear*, vol. 270, feb 2011, pp. 665–673.
45. B. Henriques, D. Soares, 2014, Effect of Hot Pressing Variables on the Microstructure, Relative Density and Hardness of Sterling Silver (Ag-Cu alloy) Powder Compacts. *Materials Research*. 2014; 17(3): pp 664-671.
46. R. German, 2005, Powder metallurgy & Particulate materials processing. *Princeton: Metal Powder Industries Federation (MPIF)*; 2005.
47. S. Montecinos, S. Tognana, D. Salgueiro, 2017, Influence of microstructure on the Young's modulus in a Cu-2Be (wt.%) alloy, *Journal of Alloys and Compounds*, (2017), doi: 10.1016/2017.09.12. pp 16-22.
48. Z. Hongtao, J. Yanbin, X. Jianxin, 2019, Precipitation behavior, microstructure and properties of aged Cu-1.7 wt% Be alloy, *Journal of Alloys and Compounds* 773 (2019) 1121e1130. pp. 1–10.

49. H. Naeem, K. Mohammad, R. Ahmad, 2014, The effect of microalloying of nickel, RRA treatment on microstructure and mechanical properties for high strength aluminum alloy. *Advanced Materials Research*. 2014; 925: pp 253-257.
50. D. Chakarbarti, E. lajughlin, L. Tranner , 1987. Cu-Be metastable solvi .1987.
51. S. Alisha, T.Venkateswaran, Effect of Heat Treatment on the Mechanical properties of Copper Beryllium alloy , *Materials Science Forum*, Vols. 830-831, 10.402/MSF.830-831.168, pp 168-171.
52. M. Mankani, S.Sharma, 2015, Heat Treatment of Mill-hardened Beryllium Copper for Space Applications, *Universal Journal of Mechanical Engineering* 3(4): 147-150, 2015,DOI: 10.13189/2015.030405, pp. 13–17.
53. Sh. Zhang, Y.Yuan, Y .Su, X. Song, 2017, Interfacial microstructure and mechanical properties of brazing carbon/carbon composites to stainless steel using diamond particles reinforced Ag-Cu-Ti brazing alloy. *Journal of Alloys and Compounds*, 15 May 2017. P 342.
54. L.Castoldi, G.Visalli , S.Morin, 2004, Copper–titanium thin film interaction, *microelectronic engineering*, Volume 76, Issues 1–4, October 2004, pp 153-159.
55. D.Paul, A.Pudney, J. Kevin, Zh.Shiping, 2009, characterizing the phase behavior of stearic acid, *Physical Chemistry Chemical Physics* · August 2009,DOI: 10.1039/b819582j, pp. 69–77.
56. G. Lu, S. Bernasek, J. Schwartz, 2000, Oxidation of a polycrystalline titanium surface by oxygen and water,” *Surface Science*, vol. 458, no. 1, 2000, pp. 85 – 90.
57. V. Ramakoteswara,N. Ramanaiah, 2016, Tribological properties of Aluminium Metal Matrix Composites(AA7075 Reinforced with Titanium Carbide (TiC) Particles), *International Journal of Advanced Science and Technology*, Vol.88 (2016), <http://dx.doi.org/10.14257/ijast.2016.88.02>. pp.13-26,
58. A. Vadiraj, M. Kamaraj, V. Sreenivasn, 2012, Effect of solid lubricants on friction and wear behaviour of alloyed gray cast iron, *Sadhana*, vol. 37, Oct 2012, pp. 569–570.

# Appendix 1



D.J. Chakrabarti, D.E. Laughlin and L.E. Tanner, 1987.

Figure.1. Cu-Be metastable phase diagrams